



HAL
open science

Endogenous *Bos taurus* RECQL is predominantly monomeric and more active than oligomers

Na-Nv Liu, Ze-Yu Song, Hai-Lei Guo, Hu Yin, Wei-Fei Chen, Yang-Xue Dai, Ben-Ge Xin, Xia Ai, Lei Ji, Qing-Man Wang, et al.

► **To cite this version:**

Na-Nv Liu, Ze-Yu Song, Hai-Lei Guo, Hu Yin, Wei-Fei Chen, et al.. Endogenous *Bos taurus* RECQL is predominantly monomeric and more active than oligomers. *Cell Reports*, 2021, 36 (10), pp.109688. 10.1016/j.celrep.2021.109688 . hal-03357276

HAL Id: hal-03357276

<https://hal.science/hal-03357276>

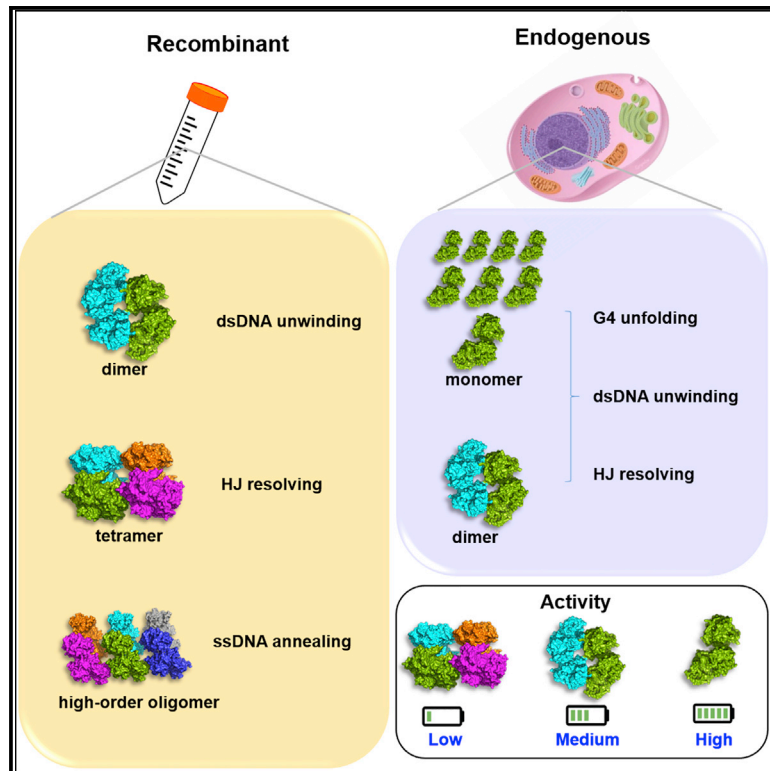
Submitted on 28 Sep 2021

HAL is a multi-disciplinary open access archive for the deposit and dissemination of scientific research documents, whether they are published or not. The documents may come from teaching and research institutions in France or abroad, or from public or private research centers.

L'archive ouverte pluridisciplinaire **HAL**, est destinée au dépôt et à la diffusion de documents scientifiques de niveau recherche, publiés ou non, émanant des établissements d'enseignement et de recherche français ou étrangers, des laboratoires publics ou privés.

Endogenous *Bos taurus* RECQL is predominantly monomeric and more active than oligomers

Graphical abstract



Authors

Na-Nv Liu, Ze-Yu Song, Hai-Lei Guo, ..., Shuo-Xing Dou, Stephane Rety, Xu-Guang Xi

Correspondence

xxi01@ens-cachan.fr

In brief

Liu et al. show that, in contrast to expectations, monomeric RECQL helicase is more abundant than oligomer/dimer forms in living cells. By measuring the binding and activity of RECQL, the authors challenge the prevailing view of the function of monomeric RECQL.

Highlights

- Endogenous RECQL exists predominantly as a monomer in bovine tissue extracts
- Endogenous and recombinant monomeric *Bt*RECQL functions effectively as a monomer
- Monomeric *Bt*RECQL unfolds intramolecular G-quadruplex DNA as efficiently as *h*BLM



Report

Endogenous *Bos taurus* RECQL is predominantly monomeric and more active than oligomers

Na-Nv Liu,^{1,6} Ze-Yu Song,^{1,6} Hai-Lei Guo,^{1,6} Hu Yin,^{1,6} Wei-Fei Chen,¹ Yang-Xue Dai,¹ Ben-Ge Xin,¹ Xia Ai,¹ Lei Ji,¹ Qing-Man Wang,¹ Xi-Miao Hou,¹ Shuo-Xing Dou,^{2,3} Stephane Rety,⁴ and Xu-Guang Xi^{1,5,7,*}

¹State Key Laboratory of Crop Stress Biology for Arid Areas, College of Life Sciences, Northwest A&F University, Yangling, Shaanxi 712100, China

²Beijing National Laboratory for Condensed Matter Physics and CAS Key Laboratory of Soft Matter Physics, Institute of Physics, Chinese Academy of Sciences, Beijing 100190, China

³School of Physical Sciences, University of Chinese Academy of Sciences, Beijing 100049, China

⁴Univ. Lyon, ENS de Lyon, Univ. Claude Bernard, CNRS UMR 5239, INSERM U1210, LBMC, 46 allée d'Italie Site Jacques Monod, F-69007, Lyon, France

⁵LBPA, Ecole Normale Supérieure Paris-Saclay, CNRS, Université Paris Saclay, Gif-sur-Yvette, France

⁶These authors contributed equally

⁷Lead contact

*Correspondence: xxi01@ens-cachan.fr

<https://doi.org/10.1016/j.celrep.2021.109688>

SUMMARY

There is broad consensus that RecQ family helicase is a high-order oligomer that dissociates into a dimer upon ATP binding. This conclusion is based mainly on studies of highly purified recombinant proteins, and the oligomeric states of RecQ helicases in living cells remain unknown. We show here that, in contrast to current models, monomeric RECQL helicase is more abundant than oligomer/dimer forms in living cells. Further characterization of endogenous *Bt*RECQL and isolated monomeric *Bt*RECQL using various approaches demonstrates that both endogenous and recombinant monomeric *Bt*RECQL effectively function as monomers, displaying higher helicase and ATPase activities than dimers and oligomers. Furthermore, monomeric *Bt*RECQL unfolds intramolecular G-quadruplex DNA as efficiently as human RECQL and BLM helicases. These discoveries have implications for understanding endogenous RECQL oligomeric structures and their regulation. It is worth revisiting oligomeric states of the other members of the RecQ family helicases in living cells.

INTRODUCTION

RecQ helicases are a ubiquitous family of DNA unwinding enzymes that play a crucial role in genome integrity and stability. During the past decades, characterization of RecQ family helicases—primarily based on purified recombinant proteins—has demonstrated that RecQ helicases adopt different quaternary forms, including higher-order oligomers (likely pentamers or hexamers) and dimers (Garcia et al., 2004; Kaiser et al., 2017; Manthei et al., 2015; Newman et al., 2015). Furthermore, members of this helicase family not only unwind duplex DNA, but also efficiently process non-canonical DNA structures, such as forked DNA, G-quadruplexes (G4), D-loops, and Holliday junction (HJ) structures (Bachrati and Hickson, 2008; Bohr, 2008; Vindigni et al., 2010).

RECQL has a unique cellular role in cell-cycle progression and/or DNA repair. In accordance with the observation that germline RECQL mutations are associated with increased susceptibility to breast cancer (Cybulski et al., 2015), its depletion

in cells results in increased frequency of spontaneous sister chromatid exchanges, chromosomal instability, and DNA damage accumulation as well as increased sensitivity to cytotoxic chemotherapy (Li et al., 2014; Sharma, 2014). In addition to its DNA 3'–5' helicase activity, RECQL can promote branch migration of HJs and duplex DNA unwinding (Popuri et al., 2008). ATP binding/hydrolysis results in the dissociation of the recombinant higher-order oligomeric/tetrameric RECQL into its dimer form (but not its monomer form) (Muzzolini et al., 2007; Sharma et al., 2005). The different activities of RECQL may be associated with distinct oligomeric forms of the protein (Muzzolini et al., 2007). Although dimers are responsible for duplex DNA unwinding activity, it has been proposed that the higher-order oligomers (hexamers or pentamers) are necessary to resolve HJ structure and catalyze strand annealing (Pike et al., 2015). RecQ family helicases may perform their activities during cellular DNA transactions in various oligomeric states. Given that the homeostatic level of intracellular ATP usually ranges from 0.5 to 5 mM (Dragon et al., 1998; Gribble et al., 2000; Kawashima, 1991;



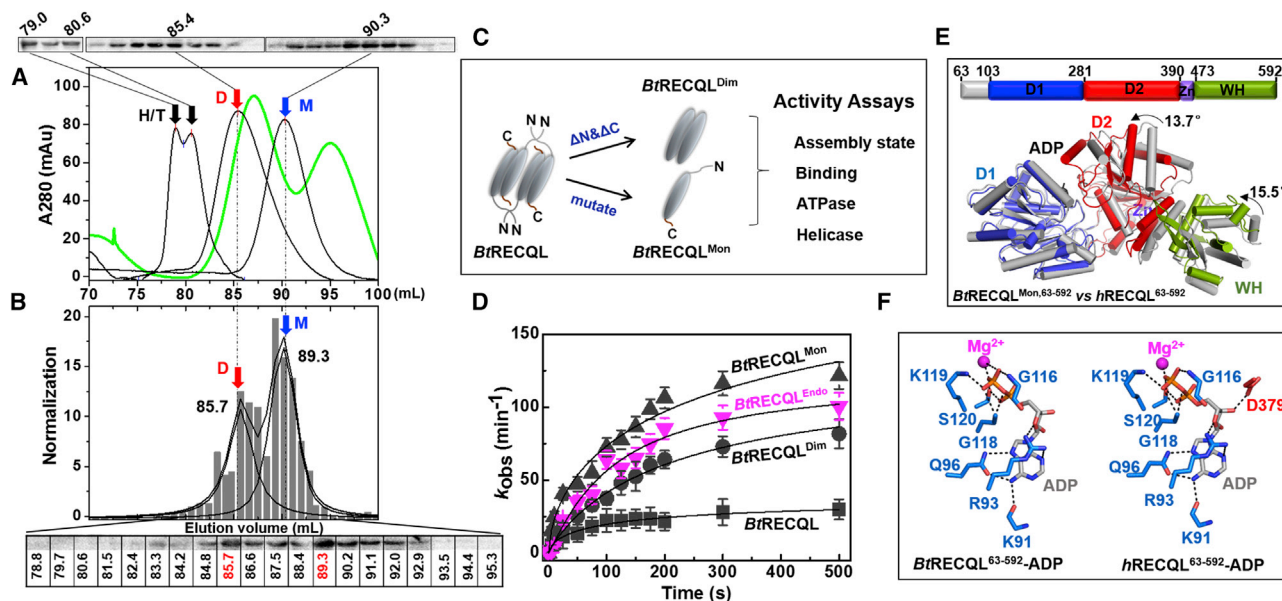


Figure 1. Monomeric RECQL is predominant in the living cell

(A) Run-through fractions of recombinant proteins (black line; H/T, D, and M represent the *BtRECQL*, *BtRECQL^{Dim}*, and *BtRECQL^{Mon}*, respectively) and whole-cell extracts (green line).

(B) The whole-cell extracts were purified using gel filtration, and all fractions were collected and recognized by RECQL antibodies and identified on western blots (bars, below); signal normalization of western blots is shown as a histogram (ImageJ software).

(C) Overview of quaternary states and activity assays explored in this study.

(D) ATPase activity of the endogenous *BtRECQL* (pink line) and different oligomeric states of recombinant *BtRECQL* (gray lines). Data are represented as mean \pm SD. The k_{cat} and K_m of endogenous *BtRECQL* were 101.9 min^{-1} and $146.3 \mu\text{M}$, respectively. Those of the different oligomeric states of recombinant *BtRECQL* are summarized in Table 1.

(E) Structural alignment between *BtRECQL^{Mon, 63-592}* (colored) and human RECQL⁶³⁻⁵⁹² (PDB entry: 2wwy, gray). See also Figures S2C and S2D.

(F) ADP binding sites in *BtRECQL^{Mon, 63-592}* and human RECQL⁶³⁻⁵⁹² (PDB entry: 2v1x).

Larcombe-McDouall et al., 1999), the distributions of oligomeric states of RECQL in cell remain completely unknown.

In this study, we characterized endogenous RECQL from bovine (*Bos taurus*) appendix tissue, which bears 90.5% identity with the human RECQL amino acid sequence, and demonstrated that the endogenous *BtRECQL* protein exists as both dimers and monomers and that the latter are more abundant than the former in cells. These observations raise the question of whether the previously revealed characteristics of RECQL using recombinantly purified forms of the protein really reflect the intrinsic properties of the RecQ family helicases in living cells.

RESULTS

Endogenous *BtRECQL* (*BtRECQL^{Endo}*) proteins exist in cells as dimers and monomers, the latter being more abundant than the former

To determine which oligomeric state of RECQL predominates in cells at physiological intracellular concentrations of ATP, a size-exclusion chromatography (SEC) column was used to characterize the elution profile of the endogenous *BtRECQL* because the native RECQL protein cannot migrate in the native gel. The endogenous *BtRECQL* proteins were prepared from the fresh cell extracts of bovine appendix tissue, and the western blot assay confirmed the presence of the endogenous *BtRECQL*

(*BtRECQL^{Endo}*) with the expected estimated molecular weight ($\approx 70 \text{ kDa}$) (Figures S1A and S1B). Meanwhile, three recombinant proteins stabilized in the tetramer, dimer, and monomer states were used as control (see below for the construction of the different oligomeric recombinant *BtRECQL*). Protein elution was first monitored at a UV absorbance at 280 nm and then analyzed in parallel using western blotting (Figures 1A and 1B). The three elution peaks of the recombinant proteins at 79.0/80.6, 85.4, and 90.3 mL correspond to the expected oligomer/tetramer, dimer, and monomer, respectively (Figure 1A, black lines), but the elution profile of the whole-cell extract enriched in endogenous *BtRECQL* is characterized by two elution peaks at 87.5 and 95.0 mL (Figure 1A, green line). The parallel western blot assay demonstrated that the endogenous protein elution produced two peaks, 85.7 and 89.3 mL, corresponding to the dimer and the monomer, respectively (Figure 1B). Taken together, these results show that in sharp contrast to previous studies with recombinant *hRECQL* proteins (Muzzolini et al., 2007), the expected higher-order oligomers are completely absent, and the dimeric and the monomeric RECQL proteins predominate in the living cell.

The purified *BtRECQL^{Endo}* displayed comparable ATPase activities (Figure 1D), and efficiently unwound duplex DNA (Figure 2A), HJs (upper panel in Figure 3E), and intramolecular G4 substrates (pink line in Figures 4B and 4D–4G) in an ATP-dependent manner. These results, presented in the next section in

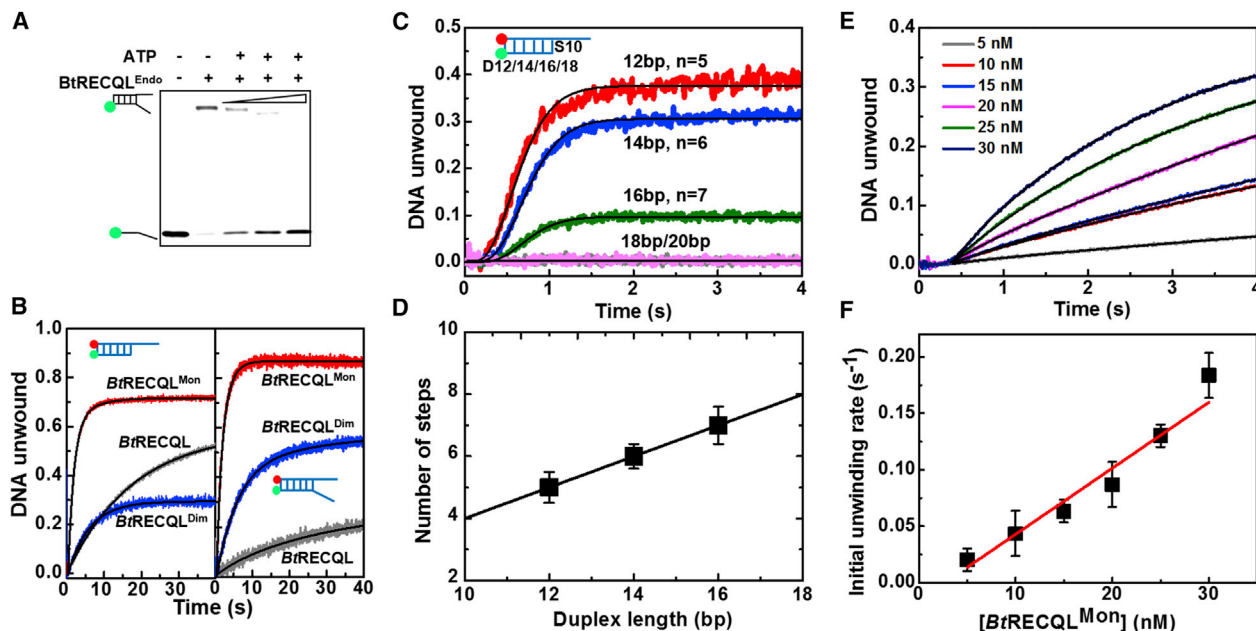


Figure 2. Duplex DNA unwinding for the endogenous *BtRECQL* and three different oligomeric states of recombinant *BtRECQL*

(A) Unwinding activity of different amounts of endogenous *BtRECQL* (1, 2, and 3 μM) on 16-bp duplexes with 10-nt 3' and 5' tails (fD16S10) analyzed using electrophoretic mobility shift assays (EMSA).

(B) Unwinding activity of 60-nM active species of three helicases on 16-bp duplex substrates with a 3' 10-nt tail (D16S10, left panel) and 16-bp duplexes with 10-nt 3' and 5' tails (fD16S10, right panel) under multiple-turnover conditions. Tetrameric *BtRECQL* is shown in gray; dimeric *BtRECQL*^{Dim} in blue, and monomeric *BtRECQL*^{Mon} in red. The solid lines are the best fits of the data to Equation 1 in STAR Methods.

(C) Kinetic time courses of single-turnover DNA unwinding of 10-nt tail ss/dsDNA of different duplex lengths. The solid lines are the best fits of the data to Equation 2 in STAR Methods, with $n = 5, 6,$ and 7 for the 12-, 14-, and 16-bp data curves, respectively.

(D) The number of steps as a function of duplex length. The line is a linear fit with a slope of 0.5 bp^{-1} , corresponding to a step size of 2 bp.

(E) The kinetic time courses at different concentrations of *BtRECQL*^{Mon} under steady-state conditions. The solid lines are double-exponential fits of the data.

(F) Initial unwinding rate (*Rate*) as a function of *BtRECQL*^{Mon} concentrations. The red line represents the linear fitting of the data points.

Data in (D) and (F) are represented as mean \pm SD.

detail, illustrate that *BtRECQL*^{Endo} is, indeed, biochemically active.

Rationale for preparation of the isolated monomeric and dimeric *BtRECQL*

Given the above results, and to conveniently characterize the monomeric *BtRECQL*, a recombinant monomeric *BtRECQL* protein was prepared. Previous studies have shown that overexpressed recombinant *hRECQL* is prone to forming stable oligomers, making it difficult to obtain high quantities of high-quality monomeric protein for enzymatic characterization. According to the crystal structure of *hRECQL*, three residues (E205, R243, and Q244) involved only in the dimeric interface were replaced with the equivalent residues bearing the same charge or similar hydrophobic groups (E205D, R243K, and Q244N). The resulting three-point-mutated protein (*BtRECQL*^{E205D/R243K/Q244N}) is—as expected—a monomer (Table S2; Figures S1G and S2A) and was named *BtRECQL*^{Mon}. Similar to previous studies, a dimeric form (*BtRECQL*^{Dim}) was constructed by truncating the first 48 residues at N-terminal regions and the last 33 amino acid residues at C-terminal regions of the full-length *BtRECQL*. The following described experiments were performed with the monomeric *BtRECQL*^{Mon}, dimeric *BtRECQL*^{Dim} and the higher-order oligomeric *BtRECQL*^{Endo} (Figure 1C), in addition to *BtRECQL*^{Endo} included as control.

Recombinant monomeric *BtRECQL*^{Mon} is fully active and well folded

We first confirmed that the higher-order *BtRECQL* oligomers dissociated into dimers upon addition of ATP, but both *BtRECQL*^{Dim} and *BtRECQL*^{Mon} remained as stable dimers and monomers, based on their molecular weights and the radius of gyration (Muzzolini et al., 2007; Sharma et al., 2005) (Table S2; Figures S1C–S1H).

A fluorescence anisotropy assay was used to assess the equilibrium DNA-binding properties of the monomeric *BtRECQL*^{Mon} compared with the tetrameric and dimeric forms of *BtRECQL* (sequences shown in Table S1). The binding affinities of the three oligomeric states of *BtRECQL* characterized on the D20S12 substrate differed by less than 1-fold in $K_{d, \text{app}}$ (Table 1; Figure S1I), indicating that the different forms of *BtRECQL* bind the D20S12 substrate with comparable affinities. Interestingly, the tetrameric protein bound to the HJ substrate with an apparent dissociation constant ($K_{d, \text{app}}$) of $139.7 \pm 1.7 \text{ nM}$, which is higher than those of the *BtRECQL* dimer ($45.8 \pm 0.5 \text{ nM}$) and monomer ($35.8 \pm 0.4 \text{ nM}$) (Table 1; Figure S1J).

The ATPase reaction catalyzed by the different oligomeric forms of *BtRECQL* in the presence of forked DNA with a 14-bp duplex DNA flanked by 18 bases of 3' and 5' single-strand DNA (ssDNA) extensions (fD14S18) was determined by a colorimetric

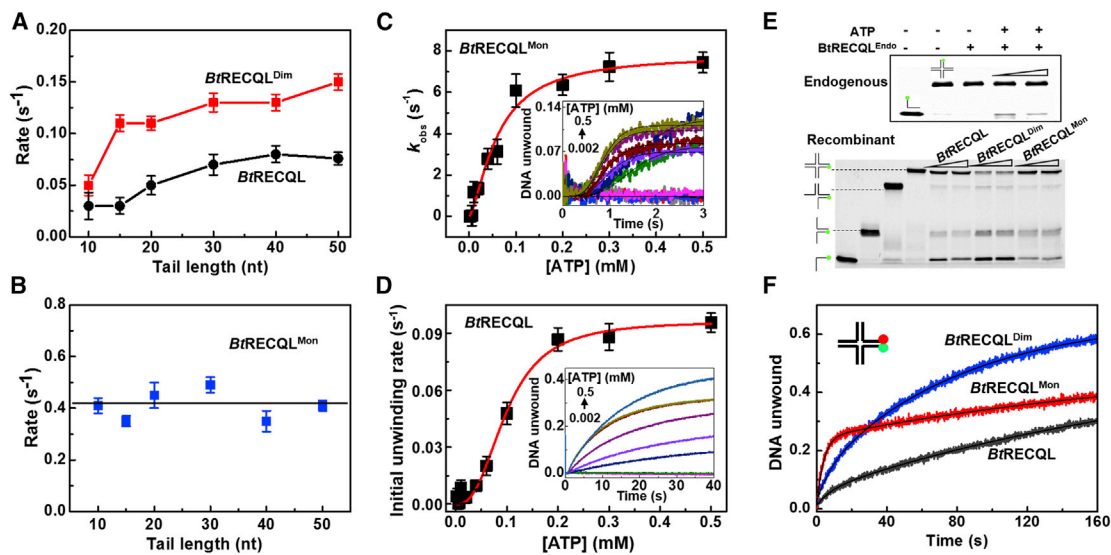


Figure 3. Different substrates are catalyzed by endogenous *BtRECQL* or different oligomeric states of recombinant *BtRECQL*

(A and B) Helicase-catalyzed DNA unwinding as a function of the length of the 3' ssDNA tail. Plots of the initial unwinding rate of *BtRECQL* (black, A), *BtRECQL*^{Dim} (red, A), and *BtRECQL*^{Mon} (blue, B) with different 3' tail lengths. Kinetic time courses are shown in Figures S1K–S1M, and the initial unwinding rate (*Rate*) and unwinding amplitude (*A_m*) are summarized in Table S3.

(C) Observed unwinding rate constant of *BtRECQL*^{Mon} with ATP concentration. The line corresponds to a best fit of the data to the Hill equation, $k_{obs} = k_{max} [ATP]^h / (K_M^h + [ATP]^h)$, where *h* is the Hill coefficient. Inset: typical kinetic time courses of single-turnover unwinding kinetics of *BtRECQL*^{Mon} at different ATP concentrations. The solid lines are best fits of the data to Equation 2 in STAR Methods, with *n* = 7.

(D) Initial unwinding rate of *BtRECQL* versus ATP concentration. Inset: typical kinetic time courses of *BtRECQL* unwinding at different ATP concentrations.

(E and F) HJ-resolving activity of endogenous *BtRECQL* (upper panel) or different oligomeric states of recombinant *BtRECQL* (lower panel) analyzed using EMSAs (E) and stopped-flow assays (F).

ATPase/GTPase activity assay kit. Both *BtRECQL*^{Endo} and *BtRECQL*^{Mon} displayed higher ATPase activities than did dimeric *BtRECQL*^{Dim} and higher oligomeric *BtRECQL* (Figure 1D; Table 1).

The crystal structure of *BtRECQL*^{Mon}, 63–592-ADP was crystallized and diffracted at 2.3 Å and harbors the canonical RecA-like domain, a zinc-binding motif, and a winged-helix (WH) domain bearing a prominent β-hairpin structure, which are highly similar to the previously solved monomeric and dimeric *hRECQL* structures (Pike et al., 2009, 2015) (Figures 1E, S2C, and S2D). Structural alignment demonstrated that the folding of the monomeric *BtRECQL*^{Mon}, 63–592 closely resembled that of apo *hRECQL* (root-mean-square deviation [RMSD] of 2.0 Å over 63–592 residues) (Pike et al., 2009) and that of a dimeric complex with DNA (RMSD of 2.9 Å over 64–593 residues) (Pike et al., 2015). Although—similarly to the *hRECQL*-ADP complex structure—ADP formed extensive contacts with domain D1 and fewer with domain D2, the D2 domain moved closer to D1 by 3 Å with a rotation of 13.7 degrees relative to *hRECQL* structures (Figures 1E and 1F). The resulting, more compact monomeric structure may facilitate ATP hydrolysis, as reported above.

Monomers are more active than dimers and tetramers in duplex DNA unwinding

Having confirmed that *BtRECQL*^{Endo} exhibits similar unwinding activity to the recombinant *BtRECQL*^{Mon} (Figure 2A), multiple-turnover unwinding kinetics experiments were carried out to compare the DNA helicase activity of *BtRECQL*^{Mon} with its dimeric and tetrameric forms. DNA unwinding was first moni-

tored by using fluorescently labeled 16-bp duplex DNA substrates possessing a 10 nt tail at its 3' end (D16S10), with donor (carboxyfluorescein, FAM) and acceptor (hexachlorofluorescein, HF) fluorophores covalently attached to each strand at the blunt end of the duplex (insert in left panel of Figure 2B; sequence is shown in Table S1). The experimental curves are fit with a double-exponential equation, and the unwinding amplitude (*A_m*) and unwinding rate (*Rate*) were derived from the fitted equation. Results showed that both *A_m* and *Rate* of the monomeric *BtRECQL*^{Mon} were higher than those of the oligomer/tetramer *BtRECQL* and dimeric *BtRECQL*^{Dim} (left panel in Figure 2B; Table S3). The experiments performed on forked duplex DNA (fD16S10) showed that the monomeric *BtRECQL*^{Mon} unwound the forked duplex DNA more efficiently than did the dimeric and the tetrameric *BtRECQL* helicases (right panel in Figure 2B; Table 1). These results demonstrate that the monomeric *BtRECQL*^{Mon} was significantly more active than dimers and tetramers on double-strand DNA (dsDNA) unwinding.

Kinetic step size and steady-state unwinding kinetics of *BtRECQL*^{Mon}

To characterize the kinetic step size of the *BtRECQL*^{Mon} helicases, single-turnover unwinding experiments were performed with partial duplex DNA substrates bearing 10-nt tails at the 3' overhang and duplex length ranging from 12 to 20 bp. As shown in Figure 2C, the unwinding kinetics curves recorded with the substrates bearing 18- and 20-bp duplexes are nearly flat, indicating that in accordance with the previous studies, the processivity of

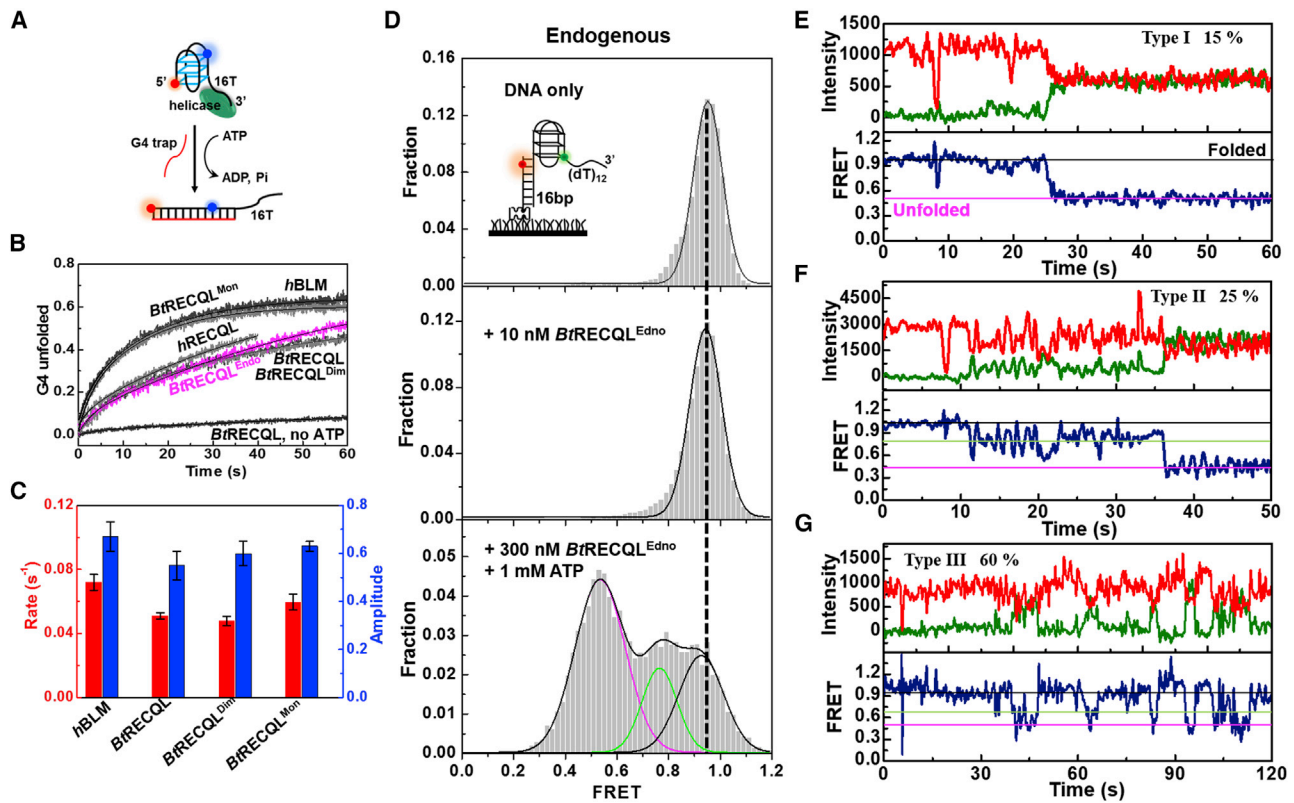


Figure 4. *BtRECQL* can catalyze G4 unfolding

(A) Schematic diagram of G4 design.
 (B) Typical kinetic time courses of G4 unfolding catalyzed by endogenous and different oligomeric states of recombinant *BtRECQL* in the absence or presence of ATP. The solid lines are the best fits of the data to Equation 1 in STAR Methods. See also Table S3.
 (C) Initial unwinding rate (*Rate*, red column) and amplitude (A_m , blue column) of tetrameric *BtRECQL*, dimeric *BtRECQL*^{Dim}, and monomeric *BtRECQL*^{Mon} unfolding of G4. A control is *hBLM* helicase unfolding of TelG4-16T under the same conditions. Data are represented as mean \pm SD.
 (D) Distribution of the FRET signal of G4 DNA catalyzed by endogenous *BtRECQL* using single-molecular FRET assays. Inset shows the schematic diagram of substrate with telomeric G4.
 (E–G) Typical FRET trajectories of G4 unwinding catalyzed by 300-nM endogenous *BtRECQL*.

BtRECQL is low. By fitting the data curves individually to Equation 2 in STAR Methods, we obtained the number of steps, n , for each duplex length L (Figure 2D). n increased linearly with duplex length according to the formula $n = (L - 2) / 2$ (Figure 2D). Therefore, the kinetic step size of *BtRECQL*^{Mon} was 2 bp, and the number of base pairs at the end of the duplex that melt spontaneously upon the approach of the helicase is also 2 bp. The corresponding average value of k_{obs} was 7.9 steps/s, and the unwinding rate was about 16 bp/s, which is lower than that of the other RecQ family helicases such as Bloom (BLM) (\sim 26 bp/s) (Xu et al., 2012; Yang et al., 2010) and *E. coli* RecQ (\sim 50 bp/s) (Zhang et al., 2008).

We then used steady-state kinetics assays to probe the oligomeric state of *BtRECQL*^{Mon} in catalysis. In the steady-state unwinding reaction, if the initial unwinding rate is linear and proportional to the helicase concentration, the protein is likely a monomer or a single and stable oligomer; otherwise, it displays non-linear dependence (sigmoidal) if oligomerization is required for unwinding. *BtRECQL*^{Mon}-mediated duplex DNA unwinding under steady-state experimental conditions was performed with 40 nM D16S10 substrate and protein concentrations

increasing from 5 to 30 nM. After incubation of *BtRECQL*^{Mon} with DNA in buffer A for 5 min at 37°C, the reaction was initiated by rapidly mixing with 1 mM ATP. Unwinding kinetics curves are given in Figure 2E, and the initial unwinding rates at each enzyme concentration were determined from the unwinding curves (Figure 2F). The initial unwinding rate (*Rate*) clearly showed linear dependence on the *BtRECQL*^{Mon} concentration, indicating that the active *BtRECQL*^{Mon} is monomeric or a single and stable oligomer during DNA catalysis.

***BtRECQL*^{Mon} unwinding efficiency is independent of ssDNA tail length**

The above results clearly show that *BtRECQL*^{Mon} possesses higher efficiency than the tetramer and dimer in duplex DNA unwinding and may function as a monomer. To further confirm that *BtRECQL*^{Mon} functions as a monomer, and not as a stable oligomer during DNA unwinding, we monitored the kinetics of DNA unwinding of 16 bp dsDNA with 3' ssDNA tail lengths ranging from 5 to 50 nt. If *BtRECQL*^{Mon} always functions as a monomer, it should be capable of unwinding all the different substrates at

Table 1. Parameters of binding, ATPase, and helicase activities determined with the three forms of *Bt*RECQL (*Bt*RECQL, tetramer; *Bt*RECQL^{Dim}, dimer; *Bt*RECQL^{Mon}, monomer)

Protein	Binding, $K_{d, app}$ (nM) ^a		ATPase ^b		Unwinding	
	D20S12	HJ	k_{cat} (min ⁻¹)	K_M (μM)	A_m	Rate (s ⁻¹)
<i>Bt</i> RECQL	17.7 ± 0.4	139.7 ± 1.7	31.2 ± 0.4	49.5 ± 1.4	0.27 ± 0.05	0.01 ± 0.01
<i>Bt</i> RECQL ^{Dim}	18.3 ± 0.7	45.8 ± 0.5	111.9 ± 2.4	156.2 ± 2.7	0.60 ± 0.03	0.08 ± 0.01
<i>Bt</i> RECQL ^{Mon}	12.9 ± 0.3	35.8 ± 0.4	148.3 ± 2.0	97.5 ± 0.3	0.91 ± 0.14	0.60 ± 0.09

The sequences of all above substrates are shown in Table S1. See also Figures S1I and S1J and Table S3.

^aThe DNA binding assays were performed with the duplex DNA substrate (D20S12) and the Holliday junction substrate (HJ).

^bThe ATPase assays were performed with a forked DNA substrate named fD16S10 or fD14S18.

similar unwinding rates, regardless of tail length. Otherwise, if functional interactions are involved in DNA unwinding, the unwinding rate would depend on substrate tail length (Yang et al., 2010). The recorded kinetic curves of three oligomeric forms of *Bt*RECQL with different ssDNA lengths are shown in Figures S1K–S1M. The unwinding rates deduced from the double-exponential fitting of the kinetic courses plotted as a function of ssDNA tail length are shown in Figures 3A and 3B. The unwinding rate of *Bt*RECQL^{Mon} was systematically higher (~0.42 s⁻¹) than those of *Bt*RECQL and *Bt*RECQL^{Dim} (0.075~0.15 s⁻¹); furthermore, the unwinding rate of *Bt*RECQL^{Mon} was independent of substrate tail length, indicating that *Bt*RECQL^{Mon} does function as a monomer during duplex DNA unwinding.

Single-turnover kinetics of DNA unwinding at varying ATP concentration further confirm the monomeric nature of *Bt*RECQL^{Mon}

ATP concentration dependence of the unwinding rate constant may provide additional information on the oligomeric state of a helicase. If the helicase functions as a monomer, the ATP concentration dependence of the unwinding rate can be described by the Hill equation with a Hill coefficient of 1; otherwise, the corresponding Hill coefficient should be different from 1 (Xu et al., 2012). The fluorescence stopped-flow assays were performed by mixing 60 nM *Bt*RECQL^{Mon} with the partial duplex DNA substrate (D16S10) and increasing ATP concentrations, ranging from 0.002 to 0.5 mM. The typical unwinding time courses are given in the insert figure of Figure 3C. We determined the ATP concentration dependence of the observed rate constant for each unwinding step (k_{obs}) (Figure 3C). The ATP concentration-dependent curve was well described by the Hill equation with a Hill coefficient equal to 1. The Hill coefficient provides an estimate of the minimum number of interacting ATP-binding sites involved in the unwinding reaction. This value is consistent with the *Bt*RECQL^{Mon} helicase utilizing only one interacting ATP-binding site during DNA unwinding. As a control, the initial unwinding rate determined with oligomeric *Bt*RECQL as a function of ATP concentration was best fit by the Hill equation, with a Hill coefficient of 2 (Figure 3D). Taken together, these data further demonstrate that *Bt*RECQL^{Mon} is a monomer during catalyzing DNA substrates.

Both dimers and monomers resolve HJs more efficiently than tetramers

To test whether *Bt*RECQL^{Endo} and *Bt*RECQL^{Mon} possess HJ-resolving activity, a 40-bp synthetic HJ substrate was prepared

following the previously described procedure and was first qualitatively analyzed using an electrophoretic mobility shift assay (EMSA). In sharp contrast with the previous observations that the *h*RECQL dimer is devoid of branch migration activity (Pike et al., 2009), we found that the dimeric *Bt*RECQL^{Dim} disrupted the HJ substrate into ssDNA products more efficiently than did the tetrameric *Bt*RECQL (lower panel in Figure 3E), and both *Bt*RECQL^{Endo} and *Bt*RECQL^{Mon} displayed significant HJ-resolving activity. The above observations are consistent with a previous study in which a purified endogenous dimeric *h*RECQL efficiently resolved HJ (LeRoy et al., 2005). To further confirm these unexpected and surprising results, the unwinding kinetics of HJ substrates were determined using fluorescence stopped-flow experiments under the same experimental conditions to determine the quantitative differences in unwinding amplitude and unwinding rate among the three assembly states. In accordance with the EMSA results, both the dimer and the monomer displayed higher unwinding amplitude (0.58 and 0.40 for the dimer and the monomer, respectively) and unwinding rates (0.02 and 0.06 s⁻¹ for the dimer and the monomer, respectively) on HJ substrates than did the tetramer *Bt*RECQL ($A_m = 0.30$ and $Rate = 0.01$ s⁻¹) (Figure 3F; Table S3). More interestingly, the unwinding rate determined from the monomer was the highest (0.06 s⁻¹). These findings are different from the previous observations with full-length *h*RECQL (Pike et al., 2009) but consistent with the HJ-resolving activity determined with a dimeric *h*RECQL purified from HeLa cell line (LeRoy et al., 2005).

Monomeric *Bt*RECQL unwinds intramolecular G-quadruplexes comparable to *h*RECQL and *h*BLM

To determine whether the monomeric *Bt*RECQL can unfold G4, we constructed an intramolecular G4 substrate consisting of human telomeric sequences and bearing a 16T ssDNA overhang at the 3' end (TelG4-16T). Two fluorescent groups, Cy3 and 6-ATTO 647N, were labeled at the 5' end and at the 19th adenine base of internal loop 2, respectively (Liu et al., 2020). Thus, the G4 folding-unfolding processes are concomitantly reflected by an increase and a decrease in the donor and acceptor emissions, respectively (Figure 4A). The G4 unfolding experiments were performed with the endogenous *Bt*RECQL^{Endo}, *h*RECQL, and *h*BLM in addition to the three oligomeric forms of the recombinant *Bt*RECQL as control. As shown in Figure 4B, in the absence of ATP, G4 unfolding was almost undetectable. Upon addition of 1 mM ATP, while both *Bt*RECQL^{Mon} and *h*BLM (the truncated BLM^{642–1290}) (Karow et al., 1997) display identical G4

unfolding activities in the levels of unfolding amplitude and unfolding rate, the other four proteins—the endogenous *BtRECQL*^{Endo}, *hRECQL*, *BtRECQL*^{Dim}, and *BtRECQL*—exhibit very similar intramolecular G4 unfolding activities, but these are lower than the isolated recombinant *BtRECQL*^{Mon} in the levels of unfolding amplitude and unfolding rate (Figure 4C).

To confirm the above results and gain mechanistic insight into the endogenous and recombinant monomeric *BtRECQL*^{Mon}-mediated G4 unfolding, we used single-molecule fluorescence resonance energy transfer (smFRET) technology to characterize the unfolding processes in more detail. As illustrated in Figure 4D (sequences shown in Table S1), the fluorophores are spaced such that the FRET signal exclusively reports the unfolding of G4, but not protein binding either to G4 or to the 3' end ssDNA tail. In the absence of ATP and protein, histograms of FRET efficiencies for G4 DNA alone showed high FRET values (~ 0.95 –1) due to the proximity of the dyes (black peak in Figure 4D).

The endogenous *BtRECQL*^{Endo}-mediated G4 unfolding assay was performed in parallel with the recombinant *BtRECQL*^{Mon} (Figures 4D–4G and S3A–S3D). Upon the addition of proteins without ATP, histograms of FRET efficiencies for G4 DNA still showed high FRET values. In the presence of the endogenous and the recombinant *BtRECQL* and 1 mM ATP, the G4 DNA was unfolded, as characterized by a decrease in the population of high FRET species and a corresponding increase in mid-FRET (~ 0.76 , green peak) and low-FRET species (~ 0.54 , pink peak), which can be attributed as the partially and completely unfolded G4 DNA, respectively (Figures 4D and S3). Of note, the high-FRET peak does not completely disappear even over 2 min, possibly due to either incomplete unfolding or refolding of unfolded G4. Inspection of the individual smFRET trajectories revealed three types of G4 unwinding kinetics (Figures 4E–4G and S3B–S3D): type I, FRET values rapidly decreased to ~ 0.54 in a single step, corresponding to complete unfolding of the G4, which accounted for 15% (Figure 4E) of the G4 substrates; and types II and III, FRET oscillated between 1 and 0.54 that lasted for more than 1 min, corresponding to repetitive unfolding and refolding, and then reached 0.45, corresponding to complete unfolding of the G4 (type II, 25%; Figure 4F) or leaped back to 0.95, corresponding to the refolded G4 (type III, 60%; Figure 4G). In conclusion, in sharp contrast to the previous studies performed with intermolecular G4, *BtRECQL* helicase efficiently unfolds intramolecular G4, and the monomer displays higher activity than do the tetrameric and dimeric proteins.

DISCUSSION

In sharp contrast to the previous observations with purified recombinant proteins, we observed no high-order oligomeric RECQL proteins in living cells, and monomers were more abundant than dimers. Why is the monomer absent in recombinant proteins and predominant in living cells? There are at least three possible scenarios. First, accessory factors may modulate oligomeric structure and activity. It has been reported that *hRECQL* is modulated by the physical and functional interactions among several proteins involved in various biological pathways (Debnath and Sharma, 2020). Other factors may also be involved. Experimentally identifying which protein modulates the RECQL

oligomeric states is needed to help elucidate the molecular mechanism by which the oligomeric states of RECQL family helicase is regulated in living cell. Second, chaperon protein factors may transiently interact with newly synthesized RECQL and maintain its monomeric nature. Third, post-translational modification (PTM) such as phosphorylation or sumoylation is one of the mechanisms by which protein conformation and function is regulated (Ababou et al., 2000; Dutertre et al., 2000; Eladad et al., 2005; Ouyang et al., 2009). Experimentally studying these possibilities and elucidating the mechanism by which the conformation of the endogenous RECQL is regulated in living cells constitutes a new research topic; we are currently working on this project.

Monomeric *BtRECQL* not only exists in cells as a major species, but also displays higher activity than dimers and oligomers. Although Lucic et al. (2011) previously prepared a monomeric *hRECQL* by introducing three mutation residues at the β -hairpin, helicase activity of this monomer was significantly impaired (Figures S4A and S4B) due to the β -hairpin being required for DNA unwinding and HJ resolution activities (Pike et al., 2009). We therefore isolated the full active monomer by introducing three residues involved only in dimerization without affecting the residues involved in catalysis and DNA binding. As expected, the crystal structure of monomeric *BtRECQL* is globally identical to those previously determined. Furthermore, we applied the steady-state and ATP-dependent kinetics approach to confirm the monomeric properties of *BtRECQL*^{Mon} during catalysis. Our extensive experiments demonstrated that monomeric *BtRECQL*^{Mon} displays unexpectedly higher ATP hydrolysis and duplex DNA unwinding activities than do dimers and oligomers. The results extend previous reports, suggesting that the monomeric form may play a more important role in cells than previously thought.

Finally, our studies reveal that the monomeric *BtRECQL* processes non-canonical DNA more efficiently than oligomers or dimers. Although a previous study suggested that only the high-order oligomeric *hRECQL* has HJ-resolution activity, we showed that both dimers and monomers are active on HJ structures, and the unwinding rate of monomers (0.06 s^{-1}) is significantly higher than those of dimeric and tetrameric *BtRECQL* (0.02 s^{-1} and 0.01 s^{-1} , respectively). Our finding in this work is fully consistent with a previous study in which a purified endogenous dimeric *hRECQL* efficiently catalyzes HJ resolution (LeRoy et al., 2005). The most surprising finding is that while it is consistent with the previous observation that *hRECQL* is deficient in intermolecular G4 unwinding (Popuri et al., 2008), both the endogenous and the recombinant *BtRECQL* helicases efficiently unfold intramolecular G4 DNA. More interestingly, monomeric *BtRECQL*^{Mon} displays the highest intramolecular G4 unfolding activity, and the efficiency is identical to *hBLM* helicase, a typical G4-unfolding RECQL family helicase. Thus, our research has solved the puzzle of why RECQL was exceptionally deficient in G4 unwinding among RECQL family helicases and may bring a new insight into the physiological significance of the observation that *hRECQL* binds to the G4 motifs, revealed by chromatin immunoprecipitation (Li et al., 2014).

What is the possible structural basis for monomeric RECQL being more active in ATP hydrolysis, duplex, and non-canonical

DNA unwinding? Inspections and comparisons of the crystal structures between the dimeric *h*RECQL and monomeric *Bt*RECQL provide two important clues. First, in monomeric *Bt*RECQL structures, the D1 and D2 domains are closer to each other than in dimeric *h*RECQL. The more compact structure between D1 and D2 likely facilitates ATP binding and hydrolysis and, consequently, provides more chemical energy that can be transferred into the mechanical unwinding force. Second, the two monomers dimerize via D1-D2' and D2-D1' in a head-to-tail manner (Figure S5). While monomeric RECQL unwinds duplex DNA and translocates along 3'–5', such dimerization conformation will restrict the translocation of each monomeric RECQL along its 3'–5' direction and, consequently, reduce the processivity unless the protein dimerization is disrupted during winding. The mechanism by which the higher-oligomer RecQ helicases are dissociated into more active monomers certainly warrants further biochemical and structural investigations.

STAR★METHODS

Detailed methods are provided in the online version of this paper and include the following:

- KEY RESOURCES TABLE
- RESOURCE AVAILABILITY
 - Lead contact
 - Materials availability
 - Data and code availability
- METHOD DETAILS
 - Reagents and buffers
 - Oligonucleotide substrates
 - Expression and purification of recombinant *Bt*RECQL
 - Extraction and purification of endogenous *Bt*RECQL from bovine appendix tissue
 - Analytical size-exclusion chromatography
 - Western blots
 - ATPase activity assay
 - Crystallization of the *Bt*RECQL^{Mon}, 63–592
 - Stopped-flow measurements
 - Single-molecular fluorescence resonance energy transfer (smFRET) assays
 - Dynamic light scattering
 - Equilibrium DNA-binding assay
- QUANTIFICATION AND STATISTICAL ANALYSIS

SUPPLEMENTAL INFORMATION

Supplemental information can be found online at <https://doi.org/10.1016/j.celrep.2021.109688>.

ACKNOWLEDGMENTS

This work was supported by the National Natural Science Foundation of China (31870788 and 32071291) and CNRS LIA (“Helicase-mediated G-quadruplex DNA unwinding and genome stability”). We thank the staff from BL17B/BL18U1/BL19U1/BL19U2 beamlines of the National Facility for Protein Science in Shanghai (NFPS) at Shanghai Synchrotron Radiation Facility for assistance during data collection. We thank Wei-wei Huang at Northwest A&F University for providing us with technical guidance on western blots; Wei Qin and Yan-Tao Yang at Northwest A&F University for preparing some proteins; and

Mei-Juan Ren at Northwest A&F University for providing us with technical guidance on MS.

AUTHOR CONTRIBUTIONS

Conceptualization, X-G.X.; methodology, X-G.X. and N-N.L.; formal analysis, N-N.L., X-G.X., and S.R.; investigation, N-N.L., Z-Y.S., H-L.G., H.Y., W-F.C., Y-X.D., B-G.X., X.A., Q-M.W., and X-M.H.; writing – original draft, X-G.X. and N-N.L.; writing – review & editing, X-G.X., S-X.D., S.R., and N-N.L.; funding acquisition, X-G.X.; resources, Z-Y.S., H.Y., and L.J.; supervision, X-G.X.

DECLARATION OF INTERESTS

The authors declare no competing interests

Received: September 21, 2020

Revised: July 11, 2021

Accepted: August 19, 2021

Published: September 7, 2021

REFERENCES

- Ababou, M., Dutertre, S., Lécluse, Y., Onclercq, R., Chatton, B., and Amor-Guéret, M. (2000). ATM-dependent phosphorylation and accumulation of endogenous BLM protein in response to ionizing radiation. *Oncogene* *19*, 5955–5963.
- Bachrati, C.Z., and Hickson, I.D. (2008). RecQ helicases: guardian angels of the DNA replication fork. *Chromosoma* *117*, 219–233.
- Bohr, V.A. (2008). Rising from the RecQ-age: the role of human RecQ helicases in genome maintenance. *Trends Biochem. Sci.* *33*, 609–620.
- Cybulski, C., Carrot-Zhang, J., Kluźniak, W., Rivera, B., Kashyap, A., Wokolorczyk, D., Giroux, S., Nadaf, J., Hamel, N., Zhang, S., et al. (2015). Germ-line RECQL mutations are associated with breast cancer susceptibility. *Nat. Genet.* *47*, 643–646.
- Debnath, S., and Sharma, S. (2020). RECQ1 Helicase in Genomic Stability and Cancer. *Genes (Basel)* *11*, 622.
- Dragon, S., Hille, R., Götz, R., and Baumann, R. (1998). Adenosine 3':5'-cyclic monophosphate (cAMP)-inducible pyrimidine 5'-nucleotidase and pyrimidine nucleotide metabolism of chick embryonic erythrocytes. *Blood* *91*, 3052–3058.
- Dutertre, S., Ababou, M., Onclercq, R., Delic, J., Chatton, B., Jaulin, C., and Amor-Guéret, M. (2000). Cell cycle regulation of the endogenous wild type Bloom's syndrome DNA helicase. *Oncogene* *19*, 2731–2738.
- Eladad, S., Ye, T.Z., Hu, P., Leversha, M., Beresten, S., Matunis, M.J., and Ellis, N.A. (2005). Intra-nuclear trafficking of the BLM helicase to DNA damage-induced foci is regulated by SUMO modification. *Hum. Mol. Genet.* *14*, 1351–1365.
- Emsley, P., and Cowtan, K. (2004). Coot: model-building tools for molecular graphics. *Acta Crystallogr. D Biol. Crystallogr.* *60*, 2126–2132.
- Garcia, P.L., Liu, Y., Jiricny, J., West, S.C., and Janscak, P. (2004). Human RECQ5beta, a protein with DNA helicase and strand-annealing activities in a single polypeptide. *EMBO J.* *23*, 2882–2891.
- Gribble, F.M., Loussouarn, G., Tucker, S.J., Zhao, C., Nichols, C.G., and Ashcroft, F.M. (2000). A novel method for measurement of submembrane ATP concentration. *J. Biol. Chem.* *275*, 30046–30049.
- Hamann, F., Enders, M., and Ficner, R. (2019). Structural basis for RNA translocation by DEAH-box ATPases. *Nucleic Acids Res.* *47*, 4349–4362.
- Hou, X.M., Wu, W.Q., Duan, X.L., Liu, N.N., Li, H.H., Fu, J., Dou, S.X., Li, M., and Xi, X.G. (2015). Molecular mechanism of G-quadruplex unwinding helicase: sequential and repetitive unfolding of G-quadruplex by Pif1 helicase. *Biochem. J.* *466*, 189–199.
- Kabsch, W. (2010). Xds. *Acta Crystallogr. D Biol. Crystallogr.* *66*, 125–132.

- Kaiser, S., Sauer, F., and Kisker, C. (2017). The structural and functional characterization of human RecQ4 reveals insights into its helicase mechanism. *Nat. Commun.* **8**, 15907.
- Karow, J.K., Chakraverty, R.K., and Hickson, I.D. (1997). The Bloom's syndrome gene product is a 3'-5' DNA helicase. *J. Biol. Chem.* **272**, 30611–30614.
- Kawashima, S. (1991). Inhibition of rat liver transglutaminase by nucleotides. *Experientia* **47**, 709–712.
- Larcombe-McDouall, J., Buttell, N., Harrison, N., and Wray, S. (1999). In vivo pH and metabolite changes during a single contraction in rat uterine smooth muscle. *J. Physiol.* **518**, 783–790.
- LeRoy, G., Carroll, R., Kyin, S., Seki, M., and Cole, M.D. (2005). Identification of RecQL1 as a Holliday junction processing enzyme in human cell lines. *Nucleic Acids Res.* **33**, 6251–6257.
- Li, X.L., Lu, X., Parvathaneni, S., Bilke, S., Zhang, H., Thangavel, S., Vindigni, A., Hara, T., Zhu, Y., Meltzer, P.S., et al. (2014). Identification of RECQ1-regulated transcriptome uncovers a role of RECQ1 in regulation of cancer cell migration and invasion. *Cell Cycle* **13**, 2431–2445.
- Liebschner, D., Afonine, P.V., Baker, M.L., Bunkóczi, G., Chen, V.B., Croll, T.I., Hintze, B., Hung, L.W., Jain, S., McCoy, A.J., et al. (2019). Macromolecular structure determination using X-rays, neutrons and electrons: recent developments in Phenix. *Acta Crystallogr. D Struct. Biol.* **75**, 861–877.
- Liu, N.N., Ji, L., Guo, Q., Dai, Y.X., Wu, W.Q., Guo, H.L., Lu, K.Y., Li, X.M., and Xi, X.G. (2020). Quantitative and real-time measurement of helicase-mediated intra-stranded G4 unfolding in bulk fluorescence stopped-flow assays. *Anal. Bioanal. Chem.* **412**, 7395–7404.
- Lu, K.Y., Chen, W.F., Rety, S., Liu, N.N., Wu, W.Q., Dai, Y.X., Li, D., Ma, H.Y., Dou, S.X., and Xi, X.G. (2018). Insights into the structural and mechanistic basis of multifunctional *S. cerevisiae* Pif1p helicase. *Nucleic Acids Res.* **46**, 1486–1500.
- Lucic, B., Zhang, Y., King, O., Mendoza-Maldonado, R., Berti, M., Niesen, F.H., Burgess-Brown, N.A., Pike, A.C.W., Cooper, C.D.O., Gileadi, O., and Vindigni, A. (2011). A prominent β -hairpin structure in the winged-helix domain of RECQ1 is required for DNA unwinding and oligomer formation. *Nucleic Acids Res.* **39**, 1703–1717.
- Manthei, K.A., Hill, M.C., Burke, J.E., Butcher, S.E., and Keck, J.L. (2015). Structural mechanisms of DNA binding and unwinding in bacterial RecQ helicases. *Proc. Natl. Acad. Sci. USA* **112**, 4292–4297.
- Muzzolini, L., Beuron, F., Patwardhan, A., Popuri, V., Cui, S., Niccolini, B., Rappas, M., Freemont, P.S., and Vindigni, A. (2007). Different quaternary structures of human RECQ1 are associated with its dual enzymatic activity. *PLoS Biol.* **5**, e20.
- Newman, J.A., Savitsky, P., Allerston, C.K., Bizard, A.H., Özer, Ö., Sarlós, K., Liu, Y., Pardon, E., Steyaert, J., Hickson, I.D., and Gileadi, O. (2015). Crystal structure of the Bloom's syndrome helicase indicates a role for the HRDC domain in conformational changes. *Nucleic Acids Res.* **43**, 5221–5235.
- Ouyang, K.J., Woo, L.L., Zhu, J., Huo, D., Matunis, M.J., and Ellis, N.A. (2009). SUMO modification regulates BLM and RAD51 interaction at damaged replication forks. *PLoS Biol.* **7**, e1000252.
- Pike, A.C.W., Shrestha, B., Popuri, V., Burgess-Brown, N., Muzzolini, L., Costantini, S., Vindigni, A., and Gileadi, O. (2009). Structure of the human RECQ1 helicase reveals a putative strand-separation pin. *Proc. Natl. Acad. Sci. USA* **106**, 1039–1044.
- Pike, A.C.W., Gomathinayagam, S., Swuec, P., Berti, M., Zhang, Y., Schnecke, C., Marino, F., von Delft, F., Renault, L., Costa, A., et al. (2015). Human RECQ1 helicase-driven DNA unwinding, annealing, and branch migration: insights from DNA complex structures. *Proc. Natl. Acad. Sci. USA* **112**, 4286–4291.
- Popuri, V., Bachrati, C.Z., Muzzolini, L., Mosedale, G., Costantini, S., Giacomini, E., Hickson, I.D., and Vindigni, A. (2008). The Human RecQ helicases, BLM and RECQ1, display distinct DNA substrate specificities. *J. Biol. Chem.* **283**, 17766–17776.
- Schneider, C.A., Rasband, W.S., and Eliceiri, K.W. (2012). NIH Image to ImageJ: 25 years of image analysis. *Nat. Methods* **9**, 671–675.
- Sharma, S. (2014). An appraisal of RECQ1 expression in cancer progression. *Front. Genet.* **5**, 426.
- Sharma, S., Sommers, J.A., Choudhary, S., Faulkner, J.K., Cui, S., Andreoli, L., Muzzolini, L., Vindigni, A., and Brosh, R.M., Jr. (2005). Biochemical analysis of the DNA unwinding and strand annealing activities catalyzed by human RECQ1. *J. Biol. Chem.* **280**, 28072–28084.
- Vindigni, A., Marino, F., and Gileadi, O. (2010). Probing the structural basis of RecQ helicase function. *Biophys. Chem.* **149**, 67–77.
- Xu, Y.N., Bazeille, N., Ding, X.Y., Lu, X.M., Wang, P.Y., Bugnard, E., Grondin, V., Dou, S.X., and Xi, X.G. (2012). Multimeric BLM is dissociated upon ATP hydrolysis and functions as monomers in resolving DNA structures. *Nucleic Acids Res.* **40**, 9802–9814.
- Yang, Y., Dou, S.X., Xu, Y.N., Bazeille, N., Wang, P.Y., Rigolet, P., Xu, H.Q., and Xi, X.G. (2010). Kinetic mechanism of DNA unwinding by the BLM helicase core and molecular basis for its low processivity. *Biochemistry* **49**, 656–668.
- Zhang, X.D., Dou, S.X., Xie, P., Hu, J.S., Wang, P.Y., and Xi, X.G. (2008). *Escherichia coli* RecQ is a rapid, efficient, and monomeric helicase. (vol 281, pg 12655, 2006). *J. Biol. Chem.* **283**, 36752.

STAR★METHODS

KEY RESOURCES TABLE

REAGENT or RESOURCE	SOURCE	IDENTIFIER
Antibodies		
Rabbit polyclonal to RECQ1 antibodies	Abcam	ab151501, RRID:AB_2892782
Rabbit monoclonal RECQL antibodies	Abcam	ab150421, RRID:AB_2892783
Bacterial and virus strains		
<i>Escherichia coli</i> BL21 (DE3) cells	NEW ENGLAND BioLabs	Cat# C25271
Biological samples		
Bovine appendix tissue	This Paper	N/D
Chemicals, peptides, and recombinant proteins		
<i>Bos taurus</i> RECQL protein	InvitrogenCorporation	Gene ID: 533006
Critical commercial assays		
Chemiluminescence kit	Beyotime Biotechnology	P0018S
ATPase activity assay kit	Sigma-Aldrich	MAK113
Deposited data		
BtRECQL ^{Mon,63-592} (apo) structure	This paper	PDB: 7A8R
Oligonucleotides		
See Table S4 for oligonucleotide information	This paper	N/A
Recombinant DNA		
See Table S1 for DNA substrates	This paper	N/A
Software and algorithms		
ImageJ	(Schneider et al., 2012)	https://imagej.nih.gov/ij/index.html
Origin 8.0	OriginLab Corporation	https://originlab-corporation.software.informer.com/

RESOURCE AVAILABILITY

Lead contact

Further information and requests for resources and reagents should be directed to and will be fulfilled by the lead contact, Xu-Guang Xi (xxi01@ens-cachan.fr).

Materials availability

Plasmids generated in this study are available upon request.

Data and code availability

- The atomic coordinates and structure factors have been deposited in the Protein Data Bank, www.wwpdb.org (PDB ID code 7A8R). Access number is listed in the [Key Resources Table](#).
- This paper does not report original code.
- Any additional information required to reanalyze the data reported in this paper is available from the lead contact upon request.

METHOD DETAILS

Reagents and buffers

All chemicals used in the present study were of reagent grade and all buffers were prepared in high-quality deionized water from a Milli-Q® ultrapure water purification system (EMD Millipore Corporation, Billerica, MA, USA) with resistivity of > 18.2 MΩ.cm; the wa-

ter was re-filtered through a 0.20 μm filter before use. All DNA-unwinding assays were performed in buffer A (30 mM Tris-HCl (pH 7.5 at 25°C), 90 mM NaCl, 3 mM MgCl_2 , and 1 mM dithiothreitol (DTT)). ATP was dissolved as a concentrated stock at pH 7.0. The ATP concentration was determined using an extinction coefficient of $1.54 \times 10^4 \text{ cm}^{-1} \text{ M}^{-1}$ at 259 nm. All chemicals were purchased from Sigma-Aldrich Corporation (St. Louis, MO, USA) unless stated otherwise.

Oligonucleotide substrates

The DNA substrates used in this study were purchased from Shanghai Sangon Biological Engineering Technology & Services Co., Ltd. (Shanghai, China). The structures and sequences are shown in [Table S1](#). All synthetic oligonucleotides were purified using high-performance liquid chromatography before storage in buffer D (10 mM Tris-HCl, pH 8.0, and 1 mM EDTA) at -20°C . Two micromolar working stocks of substrates were prepared by annealing them with equal concentrations of complementary single-stranded (ss) oligonucleotides for stopped-flow assays or with a 1:3 mixture of the stem and G4 strands for single-molecule fluorescence resonance energy transfer (FRET) measurements. After heating the mixture to 95°C for 5 min in 20 mM Tris-HCl buffer (pH 7.5 at 25°C) containing 100 mM KCl, the oligonucleotides were annealed by slowly cooling to room temperature and then stored at -20°C .

Expression and purification of recombinant BtRECQL

The gene encoding the *Bos taurus* RECQL protein (*BtRECQL*, Gene ID: 533006) was cloned into a pET21a vector (Invitrogen Corporation, Carlsbad, CA, USA). All constructs were verified using PCR screening and sequencing (Shanghai Invitrogen Biotechnology Co., Ltd., Shanghai, China). The *BtRECQL* expression vector was transformed into *Escherichia coli* BL21 (DE3) cells cultured at 37°C to an optical density of ~ 0.6 at 600 nm and then induced overnight with 0.3 mM isopropyl β -D-1-thiogalactopyranoside at 18°C . After centrifugation, the cell pellets were re-suspended in lysis buffer (20 mM Tris-HCl, pH 7.6, 500 mM NaCl, and 5 mM imidazole). The cells were sonicated and then centrifuged at 12,000 rpm for 40 min. Before loading on a HisTrap HP affinity column (GE Healthcare Life Sciences, Chicago, IL, USA), the samples were filtered through a 0.22 μm filter. The eluted fraction containing *BtRECQL* was collected and diluted in Q low-salt buffer (20 mM Tris-HCl, pH 8.0, 1 mM DTT, and 100 mM NaCl). Then the sample was loaded onto a HiTrap Q HP (GE Healthcare Life Sciences) column and eluted using the ÄKTA protein purification system (GE Healthcare Life Sciences). The pooled samples were concentrated and further purified by gel filtration using a Superdex 200 10/300 GL column (GE Healthcare Life Sciences). Each sample was polished using Mono Q ion exchange media (GE Healthcare Life Sciences). The final purified proteins were dialyzed against the storage buffer (20 mM Tris-HCl, pH 7.4, 350 mM NaCl, 1 mM DTT and 20% glycerol (v/v)) and then stored at -80°C . The procedure for the expression and purification of the truncated form of *BtRECQL* lacking the first 48 and the last 33 amino acid residues at the C terminus (called *BtRECQL*^{Dim}) and the E205D/R243K/Q244N-*BtRECQL*^{Dim} three-point mutant (also termed *BtRECQL*^{Mon}) followed that used for human RECQL described previously ([Lucic et al., 2011](#)), because the sequence identity is 90.5% between human RECQL and *BtRECQL* in sequence alignment. *BtRECQL*^{Dim} and *BtRECQL*^{Mon} were expressed and purified using the same methods used for *BtRECQL*. After purification, the purity of proteins were $\geq 95\%$ as judged by sodium dodecyl sulfate-polyacrylamide gel electrophoresis (SDS-PAGE) ([Figure S1A](#)).

Extraction and purification of endogenous BtRECQL from bovine appendix tissue

For protein extraction, 5 kg of bovine appendix tissue was diced into very small pieces of approximately 0.2 cm^3 in 1X PBS buffer, then pelleted by centrifugation ($5000 \times g$, 30 min) three times and the supernatant containing the adipose tissue was discarded. After liquid nitrogen grinding, the proteins were extracted using ultrasound-assisted extraction (300 W power output, 7 s/3 s pulses for 4 min and interval for 1 min, 10–15 cycles) with 500 mL of 10 mM sodium phosphate buffer (pH 7.4, 25°C) containing 500 mM NaCl and 2% cOmplete Protease Inhibitor Cocktail (Roche). All procedures were performed at 4°C .

The extract was clarified by centrifugation for 40 min at $12\,000 \times g$ at 4°C and solid ammonium sulfate was added to the extract to a final saturation of 60% and the mixture was stirred for an additional 2 h at 4°C . The precipitate was pelleted by centrifugation at $12\,000 \times g$ for 45 min at 4°C and the pellet was resuspended in 10 mL 10 mM sodium phosphate buffer (pH 7.4, 25°C) containing 500 mM NaCl and 2% cOmplete Protease Inhibitor Cocktail (Roche). The sample was concentrated and further purified by gel filtration using a Superdex 200 10/300 GL column (GE Healthcare Life Sciences) applied at a flow-rate of 0.3 mL/min. Protein samples were collected 0.3 mL/tube and each tube was separately concentrated 10-fold using an Amicon Ultra-15 (Millipore) with a 30 kDa MWCO membrane.

The eluted fraction containing the *BtRECQL* monomer was collected and diluted in SP buffer (50 mM Tris-HCl, pH 7.0, 1 mM DTT, 1 mM EDTA, 5% glycerol, and 70 mM NaCl). Then, the sample was loaded onto a SP column (GE Healthcare Life Sciences) and eluted with the SP elution buffer (50 mM Tris-HCl, pH 7.0, 1 mM DTT, 1 mM EDTA, 5% glycerol, and 70–500 mM NaCl concentration gradient) using the ÄKTA protein purification system (GE Healthcare Life Sciences). Fractions containing RECQL were collected and immunoprecipitated (IP) with the anti-RECQL antibody (ABCAM, ab151501), followed by confirming with mass spectrometry (Orbitrap Fusion Lumos, Thermo Fisher, USA). After purification, about 50 μg of endogenous *BtRECQL* was obtained.

Analytical size-exclusion chromatography

Gel filtration experiments were performed using a 10/30 Superdex 200 GL gel filtration column (GE Healthcare Life Sciences) as described previously ([Lu et al., 2018](#)). Briefly, the column was equilibrated at a flow rate of 0.4 mL/min with 20 mM Tris-HCl (pH 7.5), 100 mM NaCl, 1 mM MgCl_2 , 1 mM DTT. About 100 μg of protein was loaded with a final concentration of 65 μM and the

absorbance at 280 and 260 nm was recorded. The experiments were performed in 10 mM sodium phosphate buffer (pH = 7.4, 25°C) containing 500 mM NaCl.

Western blots

Proteins were resolved on 10% SDS-PAGE gels. Proteins were transferred to Immobilon-P (Millipore) probed with rabbit monoclonal RECQL antibodies (ab150421, Abcam, Cambridge, USA) in TBST buffer (20 mM Tris-HCl, pH 7.5, 150 mM NaCl and 0.2% Tween-20). After extensive washing, the blots were probed with goat anti-rabbit IgG coupled to horseradish peroxidase (Abcam). The blots were washed and developed by chemiluminescence (Beyotime Biotechnology, Shanghai, China).

ATPase activity assay

The ability of proteins to hydrolyze ATP was tested using an ATPase activity assay as previously described (Hamann et al., 2019). Briefly, 50 nM active species were tested in the presence of 1 μM forked DNA (fD14S18, sequence were shown in Table S1) and 500 μM ATP using a VICTOR Nivo Multimode Microplate Reader (PerkinElmer, Waltham, MA, USA). All reactions were performed in triplicates of 150 μL each at 25°C in buffer A. The parameters of K_m and k_{cat} were calculated by fitting the experimental data to the Michaelis–Menten equation using Origin 9.0 (OriginLab Corporation, Northampton, MA, USA).

Crystallization of the BtRECQL^{Mon, 63-592}

We initially attempted to crystallize BtRECQL^{Mon}, but were unsuccessful. A construct encompassing amino acids 63–592 of RECQL (BtRECQL^{Mon, 63-592}) was purified as previously reported (Pike et al., 2009); it was a monomer and had unwinding activity comparable to that of BtRECQL^{Mon} (Figures S2A and S2B). Crystallization screening was carried out with vapor diffusion at 20°C using commercial screening kits (Hampton Research (Aliso Viejo, USA), Molecular Dimensions (Sheffield, England) and Rigaku Reagents (Seattle, USA)). Optimized crystallization conditions included 100 mM HEPES/NaOH pH 7.0, 15% (w/v) PEG 20,000 as the precipitant solution. The X-ray diffraction data were collected on beamline BL19U-1 at the SSRF synchrotron (Shanghai, China) on a Pilatus 6M detector (Dectris, Philadelphia, PA, USA) and were processed using X-ray Detector Software (XDS) (Kabsch, 2010). Structure was solved by molecular replacement with hRECQL as model (PDB: 4U7B) using Phaser module in Phenix (Liebschner et al., 2019). Refinement was performed within Phenix with manual rebuilding with Coot (Emsley and Cowtan, 2004).

Stopped-flow measurements

The stopped-flow kinetic assays were conducted using a Bio-Logic SFM-400 mixer with a 1.5 × 1.5-mm cell (FC-15, Bio-Logic Science Instruments, Seyssinet-Pariset, France), and a Bio-Logic MOS450/AF-CD optical system equipped with a 150 W mercury-xenon lamp. For the dsDNA-unwinding kinetic assays, 6-carboxyfluorescein was excited at a wavelength of 492 nm (2 nm slit width), and its emission was monitored at 525 nm using a high-pass filter with a 20 nm bandwidth (D525/20; Chroma Technology Corporation, Bellows Falls, VT, USA). To convert the output data from volts to fractions of unwound dsDNA, calibration experiments were performed as described elsewhere. For the G4 unfolding kinetics assays, a constructed substrate that has a 16T overhang at the 3' end (TelG4-16T, 8 nM) was used. The G4 trap is a complete sequence complementary to G4 to prevent the unfolded G4 from refolding. Cy3 was excited at a wavelength of 530 nm (2 nm slit width), and its emission was monitored at 568 nm using a high-pass filter with a 30 nm bandwidth (D568/30; Chroma Technology Corporation) (Liu et al., 2020). All kinetic assays were measured in a two-syringe mode. The reacting agents were separately pre-incubated in reaction buffer A in two syringes, and the reaction was initiated by rapidly mixing them at 37°C. To convert the output data from volts to fractions of unfolded G4, calibration experiments were performed with protein, a G4 trap, ATP, and TelG4-16T which was annealed in LiCl buffer and incubated for 10 min to ensure that the reaction was complete. The fluorescent signal of the mixed solution corresponded to 100% unfolding. All solutions were filtered and extensively degassed just before use. The stopped-flow temperature was controlled using an external thermostatic water bath (Ministat 125; Peter Huber Kältemaschinenbau GmbH, Offenburg, Germany) and a high-flow pump to circulate the water between the bath and the stopped-flow apparatus. All concentrations indicated are after mixing, and the helicase concentrations refer to active species unless noted otherwise.

All stopped-flow kinetic traces are averages of more than 10 individual traces. The multiple-turnover kinetic traces were analyzed using Bio-Kine software (version 4.26, Bio-Logic Science Instruments, Seyssinet-Pariset, France) based on Equation 1:

$$A(t) = A_1(1 - e^{-k_1(t-t_0)}) + A_2(1 - e^{-k_2(t-t_0)}), \quad (\text{Equation 1})$$

where $A(t)$ is the fraction of unwound dsDNA or unfolded G4 as a function of time, A_1 and A_2 are the amplitudes of the unwound dsDNA or unfolded G4, k_1 and k_2 are the rate constants of the two phases, and t_0 is the time at which the fraction of unwound dsDNA or unfolded G4 starts to increase. From the four parameters obtained through fitting, the total amplitude of the unwound dsDNA or unfolded G4 are represented as $A_m = A_1 + A_2$ and the initial dsDNA unwinding or G4 unfolding rate (i.e., the slope of the kinetic unwinding trace at early times), $\text{Rate} = A_1k_1 + A_2k_2$.

The single-turnover kinetic traces were analyzed using Bio-Kine software (version 4.26) or based on Equation 2:

$$A(t) = A \left(1 - \sum_{r=1}^n \frac{k_{obs}^{r-1} t^{r-1}}{(r-1)!} e^{-k_{obs} t} \right), \quad (\text{Equation 2})$$

For the step size assay, a 4 nM DNA substrate was first preincubated with 60 nM active species, and the unwinding reaction was initiated by adding 1 mM ATP with 2 μ M protein trap (dT₃₀) under single-turnover conditions. For single-turnover kinetics with a negligible slow phase, Equation 2 describes the single-turnover unwinding kinetic process by a helicase in sequential n steps. A is the unwinding amplitude, whereas k_{obs} is the observed rate constant for each unwinding step.

Single-molecular fluorescence resonance energy transfer (smFRET) assays

The smFRET assays were conducted with a home-built total internal reflection fluorescence (TIRF) microscope; we used the method in Hou et al. (2015). Coverslips (Thermo Fisher Scientific, Waltham, MA, USA) and slides were cleaned thoroughly using a mixture of sulfuric acid, hydrogen peroxide, acetone, and sodium ethoxide, and the surfaces of the coverslips were then coated with a mixture of 99% monomethoxy-polyethylene glycol (m-PEG-5000; Laysan Bio, Inc., Arab, AL, USA) and 1% biotin-PEG (biotin-PEG-5000, Laysan Bio, Inc.). Streptavidin (10 μ g/mL) in buffer A was added to the microfluidic chamber composed of the slide and the PEG-coated coverslip, which was then incubated for 10 min. After washing, 50 pM G4 DNA (G4 was linked to a 16 bp duplex DNA at its 5' end and a 12 nt ssDNA at its 3' end) was added to the chamber and immobilized for 10 min. Then, free DNA was removed by washing with the imaging buffer B (30 mM Tris-HCl (pH 7.5 at 25°C), 90 mM NaCl, 3 mM MgCl₂, 1 mM DTT, 0.8% D-glucose, and 1 mg/mL glucose oxidase (266,600 U/g, Sigma-Aldrich Corporation), 0.4 mg/mL catalase (2000–5000 U/mg, Sigma-Aldrich) and 4 mM Trolox). Imaging was initiated before *Bt*RECQL^{Mon} and ATP were flowed into the chamber. An exposure time of 100 ms was used for single-molecule measurements at a constant temperature of 22°C. FRET efficiency was calculated as $I_A / (I_D + I_A)$, where I_D and I_A represent the intensity of the donor and acceptor, respectively. FRET values above 1 are due to background subtraction from a very low intensity in the donor channel, producing negative donor intensity. Basic data analysis was performed using scripts written in MATLAB, and all data fittings were generated with Origin 9.0 analysis and graphing software. The smFRET histograms were generated by picking the initial 50–100 frames of each trace from \sim 300 molecules, and fitted to multi-peak Gaussian distributions, with the peak position unconstrained.

Dynamic light scattering

Dynamic light scattering (DLS) measurements were performed using a DynaPro NanoStar instrument (Wyatt Technology Corporation, Goleta, CA, USA) with a 50 μ L cuvette. Scattered light was collected at an angle of 90°. Buffer A was used for measuring. Protein concentrations were 5.0 μ M. A total of 0.1 mL of filtered solution was incubated for 5 min at room temperature before data collecting. Recording times were typically between 3–5 min (20–30 cycles at an average of 10 s each). Data were analyzed using the Dynamics v7.0 software. The molecular weight (Mw) was calculated from the hydrodynamic radius using the following empirical equation :

$$Mw = (1.68 \times R_H)^{2.34}, \quad (\text{Equation 3})$$

Where Mw and R_H represent the molecular weight (in kDa) and the hydrodynamic radius (in nm), respectively.

Equilibrium DNA-binding assay

The binding of *Bt*RECQL to fluorescein-labeled DNA substrates was analyzed using a fluorescence polarization assay on an Infinite F200 instrument (TECAN, Switzerland). Briefly, varying amounts of protein were added to a 150 μ L solution of buffer A containing 5 nM fluorescein-labeled DNA. Each sample was allowed to equilibrate in solution for 5 min. After 5 min, the steady-state fluorescence anisotropy (r) was measured.

QUANTIFICATION AND STATISTICAL ANALYSIS

All graphs represent mean values \pm SD. Statistical differences were calculated according to nonparametric tests. The numbers of measurements (n), mean values and standard deviations (SD) were reported along the figure legends. Statistical analysis was computed using Origin 9.0 (OriginLab Corporation, Northampton, MA, USA).

Cell Reports, Volume 36

Supplemental information

Endogenous *Bos taurus* RECQL

is predominantly monomeric

and more active than oligomers

Na-Nv Liu, Ze-Yu Song, Hai-Lei Guo, Hu Yin, Wei-Fei Chen, Yang-Xue Dai, Ben-Ge Xin, Xia Ai, Lei Ji, Qing-Man Wang, Xi-Miao Hou, Shuo-Xing Dou, Stephane Rety, and Xu-Guang Xi

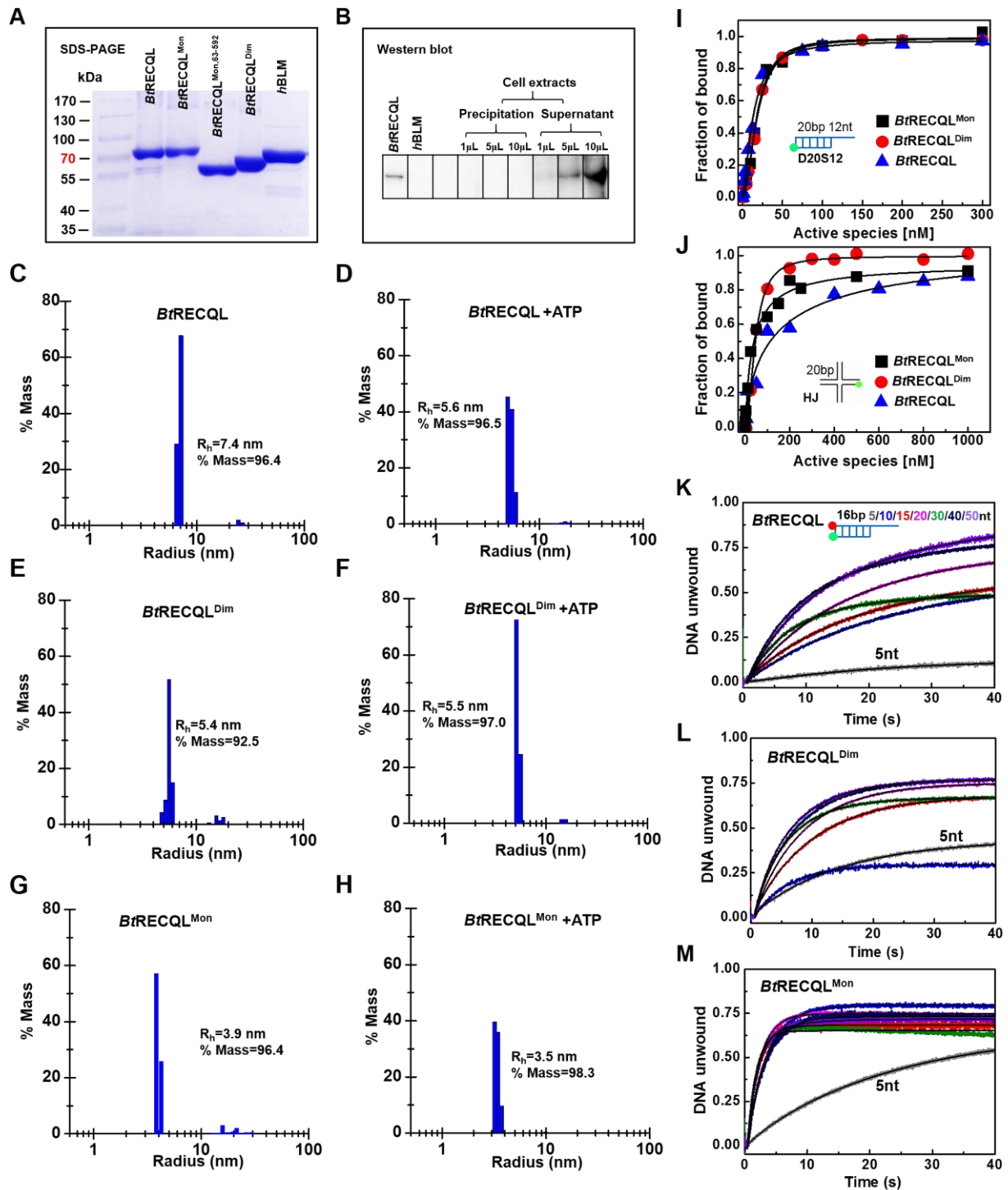


Figure S1. The radii and helicase-catalyzed DNA activities of different oligomeric states of *BtRECQL*. Related to Figures 1, 3A and 3B.

(A) SDS-PAGE analyses of the purified nuclear form of *BtRECQL* proteins and its mutant proteins. 20 μ g of protein was loaded onto a 10 % polyacrylamide gel.

(B) Western blot experiments performed with proteins from the cellular extracts in parallel with the recombinant proteins *BtRECQL* and *hBLM*. ~100 ng *BtRECQL* and *hBLM* were loaded on 10 % SDS PAGE.

(C–H) Radius distributions of the different oligomeric states of *BtRECQL* in the absence and presence of ATP, obtained from dynamic light scattering measurements. All the determined parameters are summarized in

Table S2.

(I, J) Equilibrium DNA-binding properties of the monomeric $BtRECQL^{Mon}$ compared with the tetrameric ($BtRECQL$) and dimeric ($BtRECQL^{Dim}$) forms of $BtRECQL$ helicase. The active species concentration-dependent changes in fluorescence anisotropy were measured with substrate D20S12 (**I**) and a Holliday junction substrate (HJ) (**J**). All the apparent dissociation constants ($K_{d, app}$) are summarized in Table 1.

(K–M) Helicase-catalyzed DNA unwinding as a function of the length of the 3' ssDNA tail under multiple-turnover conditions. The kinetic time-courses of 240 nM tetrameric $BtRECQL$ (60 nM active species) (**K**), 120 nM dimeric $BtRECQL^{Dim}$ (60 nM active species) (**L**), and 60 nM monomeric $BtRECQL^{Mon}$ (60 nM active species) (**M**). The 16 bp duplex with a 3' ssDNA tail of length from 5 to 50 nt. The solid lines were fitted to Equation 1.

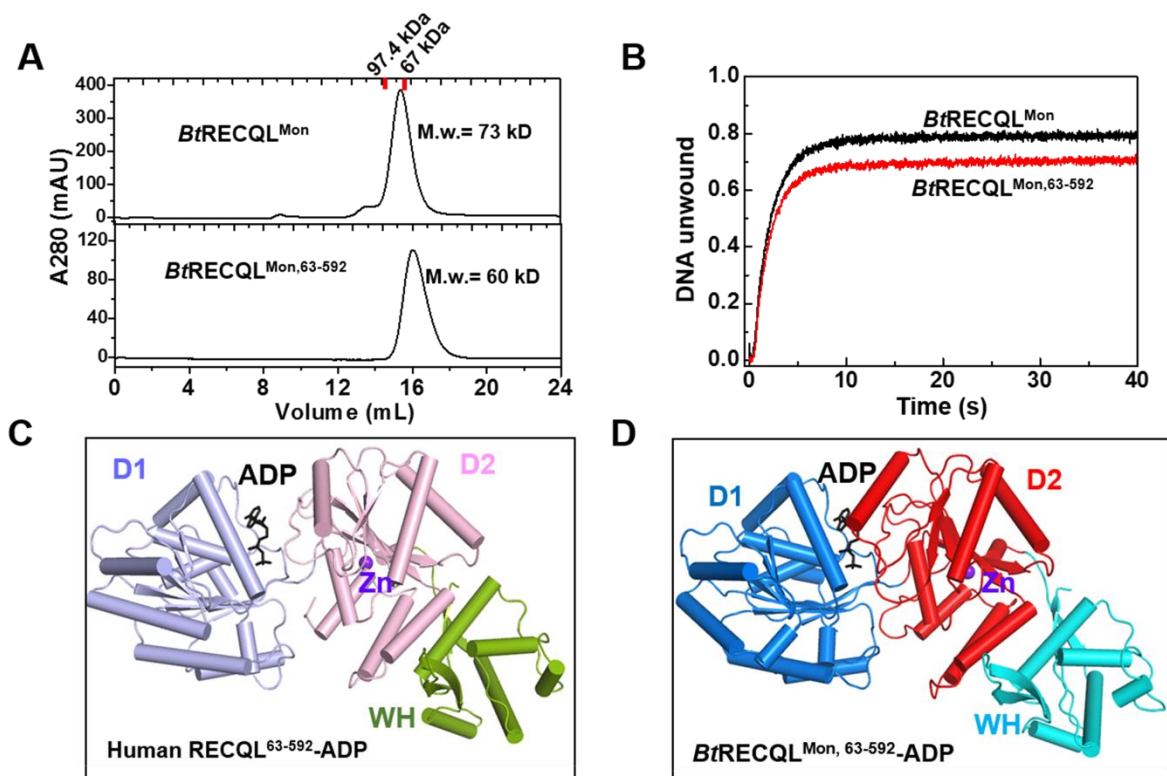


Figure S2. Crystal structure of *BtRECQL*^{Mon, 63-592}. Related to Figure 1E.

(A) Size-exclusion chromatography analysis of *BtRECQL*^{Mon} and *BtRECQL*^{Mon, 63-592} on a Superdex200 10/300 GL column. The column was equilibrated at a flow rate of 0.4 mL/min with 10 mM HEPES (pH 7.5), 100 mM KCl, 5 mM MgCl₂. About 10 μM proteins were loaded and absorbance at 280 and 260 nm was recorded at 25 °C. At the same time, albumin (67 kDa) and phosphorylase b (97.4 kDa) were loaded under the same conditions as external standards. (B) Kinetic time-courses of DNA unwinding for *BtRECQL*^{Mon} and *BtRECQL*^{Mon, 63-592} under multiple-turnover conditions. (C) Crystal structure of human RECQL⁶³⁻⁵⁹² (PDB entry: 2wvy). (D) Crystal structure of *BtRECQL*^{Mon, 63-592}.

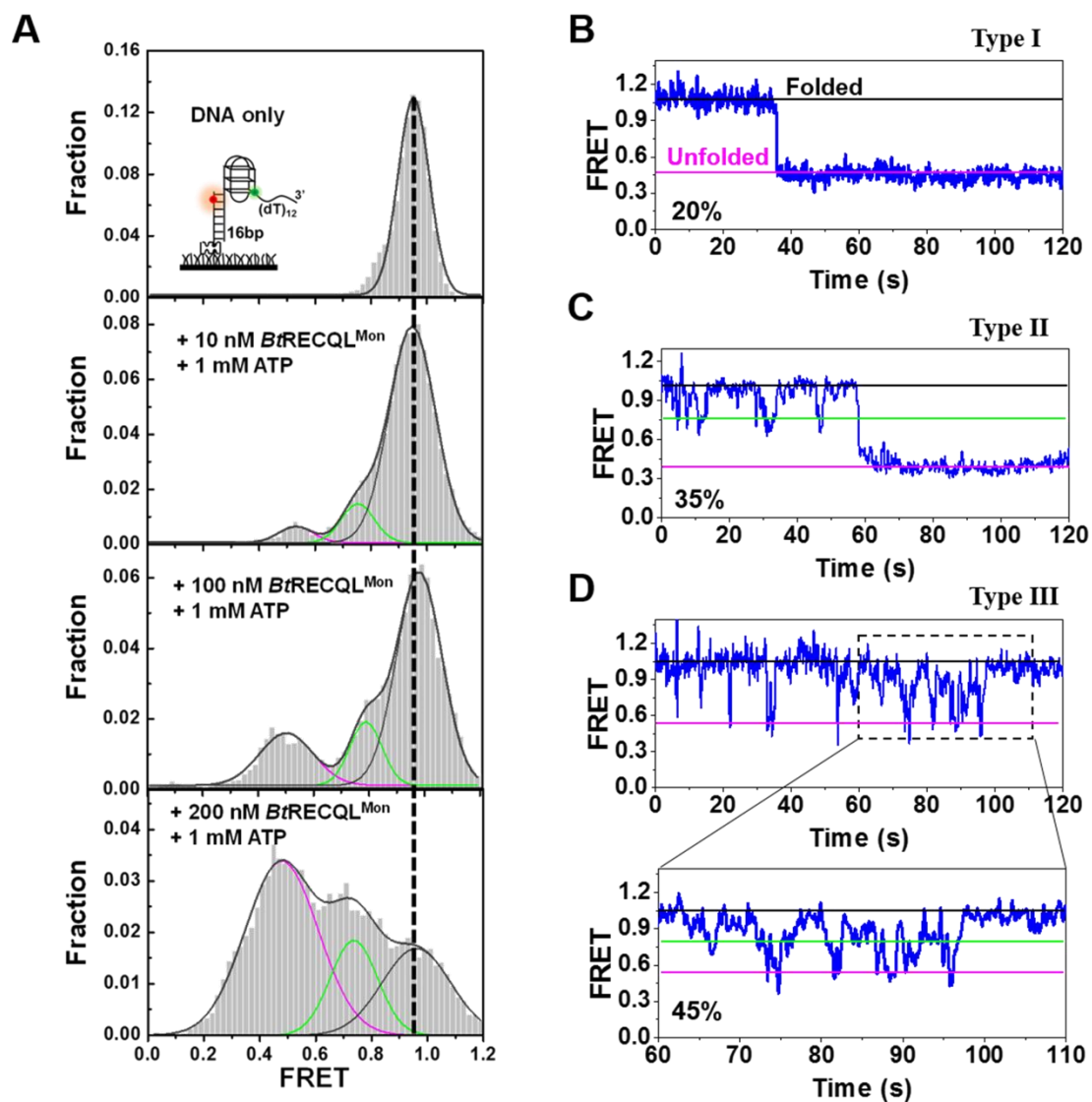


Figure S3. *BtRECQL* monomers can catalyze G4 unfolding. Related to Figures 4D–4G.

(A) Distribution of the FRET signal at different concentrations of *BtRECQL*^{Mon} using smFRET assays. The concentrations of *BtRECQL*^{Mon} were 0, 10, 100, and 200 nM. Insert figure shows the schematic diagram of the substrate with telomeric G4. G4 was linked to a 16-bp duplex DNA at its 5' end and a 12-nt ssDNA at its 3' end. Upon addition of *BtRECQL*^{Mon} and ATP (1 mM), the G4 DNA was unfolded, as characterized by a decrease in the population of high FRET species and a corresponding increase in mid-FRET (~0.74, green peak) and low-FRET species (~0.48, pink peak), which can be attributed as the partially and completely unfolded G4 DNA, respectively.

(B–D) Typical FRET trajectories of G4 unwinding catalyzed by 200 nM *BtRECQL*^{Mon}. Inspection of the individual smFRET trajectories revealed three types of G4 unwinding kinetics: Type I, FRET values rapidly decreased to ~0.48 in one single step, corresponding to the complete unfolding of the G4, which accounted for 20% of the G4 substrate (B); Types II and III, FRET oscillated between 1 and ~0.48 that lasted for more than 1 min, corresponding to repetitive unfolding and refolding, and then reached ~0.35, corresponding to complete unfolding of the G4 (Type II, 35%) (C) or leaped back to 0.95, corresponding to the refolded G4 (Type III, 45%) (D).

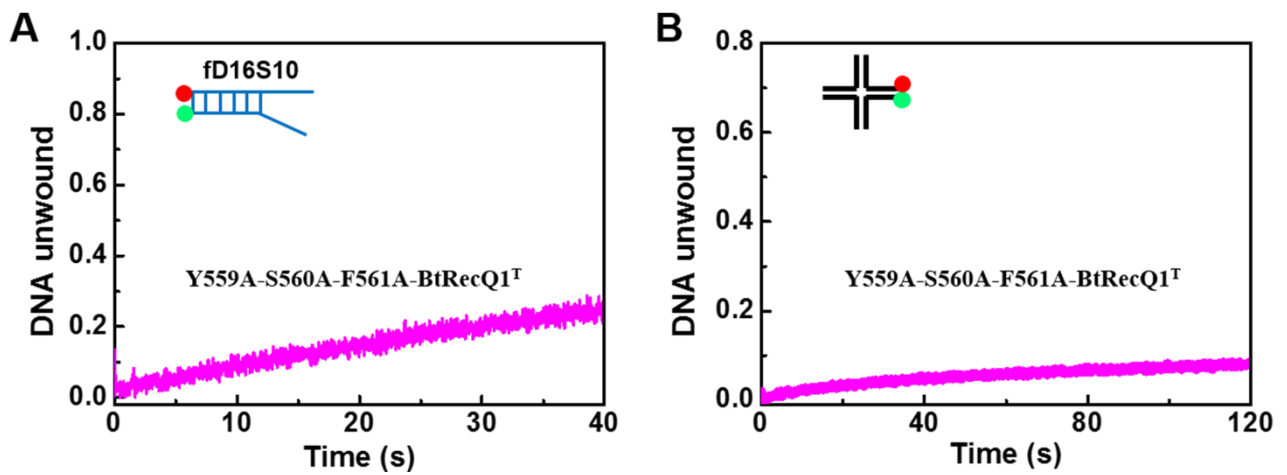


Figure S4. The β -hairpin is required for DNA unwinding. Related to Figure 2B.

Unwinding kinetics time-courses of forked DNA (A) and Holliday junction DNA (B) for Y559A-S560A-F561A-BtRecQ1^T under multiple-turnover conditions. The three mutation residues Y559A, S560A, and F561A are located at the β -hairpin (see Lucic *et al.*, 2010).

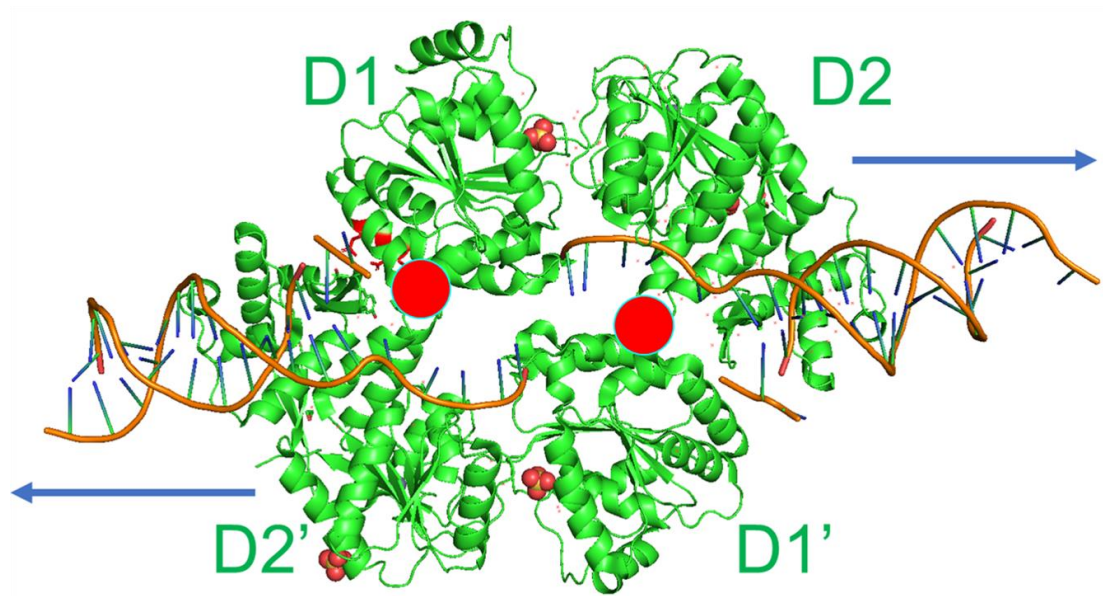


Figure S5. Dimeric *h*RECQL structure (PDB entry: 2wwy). Related to Figure 1E.

Two antiparallel monomers dimerize at D1-D2' and D2-D1', and translocations of the two monomers in opposite directions are restricted.

Table S1. DNA substrates used in DNA binding and unwinding assays. Related to Figures 1D and 2–4.

Substrate	Sequence (5'–3')
For DNA unwinding	
16 bp duplex with varying 3' ssDNA tail	CTCTGCTCGACGGATT-F ^a H ^b -AATCCGTCGAGCAGAG(dT _N)
fD16S10	(dT ₁₀)CTCTGCTCGACGGATT-F H-AATCCGTCGAGCAGAG(dT ₁₀)
DNA trap	CTCTGCTCGACGGATT
smS ₁₂ G4D ₁₆	AATCCGTCGAGCAGAGTTGGGTTAGGGTAAGGGTTAGGGT(iCy3)TTTTT TTTTTT CTCT(iCy5)GCTCGACGGATT
TelG4-16T	Cy3-AGGGTTAGGGTTAGGGTT ₆ ^c GGGTTTTTTTTTTTTTTTTT
G4 trap	CCCTAACCCCTAACCCCTAACCCCT
Protein trap	dT ₃₀
For DNA binding	
D20S12	CACTGGCCGTCTTACGGTCGCTCTGCTCGACG-F CGACCGTAAGACGGCCAGTG
Holliday junction (HJ)	ACGTGGGCAAAGGTAGCAGTTACCTGTGACAGCTGCATGG CCGTGATCACCAATGCAGATTGACGAACCTTTGCCACGT CCATGCAGCTGTCAGTCCATTGTCATGCTAGGCCTACTGC-F (H-)*GCAGTAGGCCTAGCATCTGTTAGAGCATTGGTGATCACGG
For ATPase	
fD14S18	ACGTGGGCAAAGGTTTTTTTGACAGCTGCATGG CCGTGATCACCAATTTTTTACCTTTGCCACGT

^a F, fluorescein; ^b H, hexachlorofluorescein; ^c 6, ATTO 647N;

* Hexachlorofluorescein labeled for Holliday junction unwinding.

Table S2. Oligomeric states of *Bt*RECQL in the absence and presence of ATP*. Related to Figures S1C–S1H.

Protein	Parameters		
	% Mass	Radius (nm)	Calculated kDa ^a / OS ^b
<i>Bt</i> RECQL	96.4 ± 0.15	7.42 ± 0.07	366 / 4~5
<i>Bt</i> RECQL + ATP	96.5 ± 0.12	5.60 ± 0.06	181 / 2
<i>Bt</i> RECQL ^{Dim}	92.5 ± 0.08	5.43 ± 0.12	158 / 2
<i>Bt</i> RECQL ^{Dim} + ATP	97.0 ± 0.09	5.50 ± 0.09	172 / 2
<i>Bt</i> RECQL ^{Mon}	96.4 ± 0.14	3.90 ± 0.07	79 / 1
<i>Bt</i> RECQL ^{Mon} + ATP	98.3 ± 0.11	3.51 ± 0.08	66 / 1

^a The theoretical molecular weights of *Bt*RECQL and *Bt*RECQL^{Dim} are ~73 and 65 kDa, respectively;

^b OS, oligomeric state;

* The assays were determined using dynamic light scattering measurements; see the text.

Table S3. Unwinding parameters of helicases with different substrates. Related to Figures 2B, 3A, 3B, 3F, and 4B.

	<i>Bt</i> RECQL [*]		<i>Bt</i> RECQL ^{Dim}		<i>Bt</i> RECQL ^{Mon}	
	<i>A_m</i>	Rate (s ⁻¹)	<i>A_m</i>	Rate (s ⁻¹)	<i>A_m</i>	Rate (s ⁻¹)
D16S5	0.14*	0.01	0.42	0.04	0.66	0.03
D16S10	0.57	0.03	0.29	0.05	0.72	0.41
D16S15	0.59	0.03	0.67	0.11	0.80	0.35
D16S20	0.76	0.05	0.74	0.11	0.77	0.45
D16S30	0.51	0.08	0.66	0.13	0.68	0.49
D16S40	0.82	0.08	0.75	0.13	0.76	0.35
D16S50	0.67	0.05	0.75	0.15	0.72	0.41
fD16S10	0.27	0.01	0.60	0.08	0.91	0.60
TelG4-16T	0.55	0.04	0.60	0.03	0.63	0.08
HJ	0.30	0.01	0.58	0.02	0.40	0.06

**Bt*RECQL, the full-length of *Bos taurus* RECQL protein;

*Bt*RECQL^{Dim}, the truncated form of *Bt*RECQL lacking the first 48 and the last 33 amino acid residues at the C-terminus;

*Bt*RECQL^{Mon}, the three-point-mutated protein of *Bt*RECQL (*Bt*RECQL^{E205D/R243K/Q244N}).

All data represent the average calculated from three measurements shown in Figures 2B, Figures 3A and 3B for dsDNA substrate, Figure 4B for substrate TelG4-16T, and Figure 3F for the Holliday junction (HJ) substrate.

Table S4. The primers information for the recombinant protein. Related to the STAR Methods.

Name	Sequence (5'–3')
Primers for BtRECQL^{Dim}	
49 Forward primer	gcgaattccatatgtgcctggaagatagcgatgcgggcgaaag
616 Reverse primer	ccgctcgagttagtcgacttcttcggtttttgttggtgccttc
Primers for BtRECQL^{Mon}	
FL Forward primer	gcgaattccatatggcgagcattagcgcgctgagcgaa
FL Reverse primer	ccgctcgagttagtcgactcaatcttcggtttttcgcgccg
E205D Forward primer	atgagccgcctggataaagcgtatgaa
E205D Reverse primer	ttcatacgctttatccaggcggctcat
R243K/Q224N Forward primer	ggcattctgaaaaaaaaactttccgaacgcg
R243K/Q224N Reverse primer	cgcgttcggaaagtttttttcagaatgcc
Primers for BtRECQL^{Mon, 63-592}	
63 Forward primer	ccgaattcagcagcccggcgagctggaacaaagaa
592 Reverse primer	ggctcgagttatttttcacgcgcatggtaatcacatg
E205D Forward primer	atgagccgcctggataaagcgtatgaa
E205D Reverse primer	ttcatacgctttatccaggcggctcat
R243K/Q224N Forward primer	ggcattctgaaaaaaaaactttccgaacgcg
R243K/Q224N Reverse primer	cgcgttcggaaagtttttttcagaatgcc